Earth and Planetary Science Letters 603 (2023) 117983

Contents lists available at ScienceDirect

Earth and Planetary Science Letters

journal homepage: www.elsevier.com/locate/epsl

Pulse-like ruptures, seismic swarms, and tremorgenic slow-slip events with thermally activated friction

Binhao Wang *, Sylvain Barbot

Department of Earth Sciences, University of Southern California, 3651 Trousdale Pkwy, Los Angeles, CA 90089, USA

ARTICLE INFO

Article history:
Received 31 July 2022
Received in revised form 21 November 2022
Accepted 27 December 2022
Available online xxxx
Editor: R. Bendick

Keywords:
thermally activated friction
earthquake cycle
crack- and pulse-like rupture
seismic swarms
slow-slip events and tremors
scaling law

ABSTRACT

The evolution of frictional resistance on a fault affects the characteristics of seismic ruptures. A wide range of rupture styles, from slow-slip events to fast earthquakes, can be explained under the isothermal rate- and state-dependent friction framework. However, laboratory experiments indicate that friction also depends on temperature, with a largely unknown impact on rupture patterns. Here, we explore how thermally activated friction affects rupture behavior in quasi-dynamic models of seismic cycles with a single velocity-weakening, temperature-strengthening asperity, whereby frictional healing occurs behind the rupture front due to shear heating. A transition from crack-like to pulse-like rupture propagation with self-healing fronts occurs as the temperature strengthening effect increases, spontaneously inducing steady, decaying, or growing pulses. With increasing activation energy, the cycle turns into earthquake swarms and tremorgenic slow-slip events, both characterized by strong interactions between slow and fast ruptures. The temperature sensitivity of friction may contribute to the natural complexity of the seismic phenomenon, potentially explaining a much wider spectrum of rupture behaviors and recurrence patterns.

1. Introduction

A wide spectrum of fault dynamics has been observed in various tectonic settings, including seismogenic and aseismic slow-slip events (e.g., Dragert et al., 2001; Shelly et al., 2006; Obara and Kato, 2016), earthquake swarms (e.g., Mogi, 1963; Sykes, 1970; Vidale and Shearer, 2006), and large earthquakes with various rupture propagation styles, including crack-like growth and self-healing pulses (e.g., Ross et al., 2020; Chen et al., 2020). One of the fundamental goals of earthquake physics is to identify the constitutive laws and physical conditions that enable this wide range of behaviors in connection with the tectonic setting.

The nucleation and propagation of slow-slip events and earthquakes can be explained in the framework of rate- and state-dependent friction in isothermal condition. Aseismic slow-slip events can be produced for a wide range of frictional properties promoting stable weakening (Ruina, 1983; Liu and Rice, 2007; Barbot, 2019b), particularly in near-neutral, velocity-weakening conditions (Nie and Barbot, 2021). Reciprocally, regular fast earthquakes spontaneously occur on unstable faults when the asperity is larger than a characteristic nucleation size (Ruina, 1983; Rice and Ruina, 1983; Gu et al., 1984; Ranjith and Rice, 1999). The fault properties also control whether the ruptures will propagate crack-like, or as a steady, growing, or decaying pulse (e.g., Idini and Ampuero, 2020; Nie and Barbot, 2022). During crack-like rupture propagation, virtually the entire region behind the rupture front slips until the arrest of the rupture, resulting in a rise time comparable to the full event duration. During pulse-like rupture propagation, the slipping region is confined to a small region trailing behind the rupture front, impacting radiation efficiency (Wang and Day, 2017; Lambert et al., 2021) and ground motion (Strasser and Bommer, 2009).

In contrast, several widely observed seismic phenomena remain poorly understood. That is the case for earthquake swarms (e.g., De Barros et al., 2020), i.e., clusters of seismicity without a characteristic mainshock that do not follow Omori's law of aftershocks. Seismic swarms often occur within regions with active hydrothermal circulation, such as volcanic zones (Mogi, 1963; Benoit and McNutt, 1996; Enomoto et al., 2017), oceanic transforms (Sykes, 1970; Roland and McGuire, 2009), and subduction zones (Nishikawa and Ide, 2017), and have been attributed to the interaction of asperities with surrounding fluids and fault creep (Vidale and Shearer, 2006; Goebel et al., 2016; De Barros et al., 2020). However, some earthquake swarms occur without the assistance of fluids (Lohman and McGuire, 2007; Roland and McGuire, 2009) and provide a proxy for the progression of fault slip (Ross and Cochran, 2021). Cur-

* Corresponding author.
E-mail address: binhaowa@usc.edu (B. Wang).

https://doi.org/10.1016/j.epsl.2022.117983
0012-821X/

rent models of seismic swarms invoke a modulation of frictional strength by pore-fluid pressure in isothermal conditions (Zhu et al., 2020; Dublanchet and De Barros, 2021). Another poorly understood phenomenon is tremorgenic slow-slip events, which combine slow and fast ruptures during a single event (Dragert et al., 2001; Shelly et al., 2006; Houston et al., 2011). Slow-slip events are in fact always associated with bursts of low-frequency earthquakes or tremors and are never entirely aseismic (Veedu and Barbot, 2016; Baba et al., 2018; Toh et al., 2018; Rousset et al., 2019a,b). Current models of tremor generation (Luo and Ampuero, 2018; Luo and Liu, 2019; Nie and Barbot, 2021) resort to frictional heterogenities to combine seismic and aseismic slip in a single event, and the possible rheological control remains unknown.

Here, we explore to what extent the wide range of fault slip behaviors can be explained by a rheological effect considering the fault frictional response in non-isothermal conditions. Laboratory experiments indicate that friction is a thermally activated process (Chester and Higgs, 1992; Chester, 1994, 1995; Heslot et al., 1994; Nakatani, 2001; Coble et al., 2014; French et al., 2015; Barbot, 2022). At steady-state, the temperature dependence can be temperature-strengthening, temperature-weakening, or temperature-neutral, similar to the velocity dependence. As shear heating raises the fault temperature during coseismic slip (Andrews, 2002; Kanamori and Brodsky, 2004; Rice, 2006), the temperature dependence of the frictional resistance enables a feedback mechanism that can affect the rupture style (Bizzarri, 2010) and the timing of earthquake nucleation (Kato, 2001). The temperature dependence also affords another weakening mechanism, such that velocity-strengthening faults can generate thermal instabilities manifested as slow-slip events (Wang and Barbot, 2020). The thermal activation of various healing mechanisms may explain the transition from velocity-strengthening to velocity-weakening with increasing temperature (Barbot, 2022).

The goal of this study is to explore how the coupling between shear heating and thermally activated friction affects rupture dynamics in a steady-state velocity-weakening, temperature-strengthening region during seismic cycles. In the next section, we describe the constitutive framework and the governing equations of the dynamic system. We perform a dimensional analysis highlighting several non-dimensional numbers of interest. In subsequent sections, we document the impact of the fault thermodynamic properties on the rupture style and recurrence patterns using the quasi-dynamic approximation with radiation damping. We find a transition from crack-like to pulse-like rupture propagation of large earthquakes as the steady-state temperature-strengthening effect enables rapid healing behind the rupture front. When the healing process is associated with larger activation energy, the seismic cycle transitions to earthquake swarms and tremorgenic slow-slip events. The temperature dependence of friction explains a wide spectrum of fault slip behaviors over seismic cycles, helping us to conceptualize the natural diversity of the seismic phenomenon.

2. Methods

2.1. Governing equations and dimensional analysis

We adopt a constitutive framework for fault slip that captures the direct weakening effect of temperature and the time-dependent healing documented in laboratory experiments (Chester and Higgs, 1992; Chester, 1994; Coble et al., 2014). First, following adhesion theory (Bowden and Tabor, 1950, 1964), we assume that the shear and normal loads are born by micro-asperities forming contact junctions at the fault interface. As a result, the real area of contact represents a small fraction of the nominal fault area, following the relationship (Barbot, 2019a)

$$\mathcal{A} = \frac{\mu_0 \bar{\sigma}}{\chi} \left(\frac{\theta V_0}{L} \right)^{\frac{b}{\mu_0}} , \tag{1}$$

where μ_0 is a reference coefficient of friction at sliding velocity V_0, χ is commensurate with the indentation hardness, and $\bar{\sigma}$ is the effective normal stress accounting for the compensating effect of pore-fluid pressure. The state variable θ approximates the age of contact, but is ultimately related to the size of the contact junctions and, therefore, can only be strictly positive. The power exponent b is small compared to 1, such that, at first approximation, the real area of contact is controlled by the effective normal stress. Next, we assume that fault slip is a thermally activated process captured by the constitutive law

$$V = V_0 \left(\frac{\tau}{\mathcal{A}\chi} \right)^{\frac{\mu_0}{a}} \exp\left[-\frac{Q}{R} \left(\frac{1}{T} - \frac{1}{T_0} \right) \right] , \tag{2}$$

where V is the slip velocity, τ is the amplitude of the shear traction vector, and a is a power exponent for the stress dependence of velocity. The Arrhenius activation depends on the activation enthalpy Q and the absolute temperature T, with the reference temperature T_0 and the universal gas constant $R = 8.314\,462\,618\,153\,24$ J/K/mol. Combining Equations (1) and (2), we obtain the rate-, state-, and temperature-dependent friction law

$$\tau = \mu_0 \bar{\sigma} \left(\frac{V}{V_0} \right)^{\frac{a}{\mu_0}} \left(\frac{\theta V_0}{L} \right)^{\frac{b}{\mu_0}} \exp\left[\frac{aQ}{\mu_0 R} \left(\frac{1}{T} - \frac{1}{T_0} \right) \right] \tag{3}$$

that shares the same Taylor series expansion in terms of $\ln(V/V_0)$ as previous formulations (Chester, 1994), but remains well-posed for vanishing velocity. The parameters μ_0, V_0, and T_0 are interdependent, such that the steady-state frictional resistance is μ_0 at sliding velocity V_0 and temperature T_0. Finally, we adopt the thermally activated evolution law

$$\dot{\theta} = \exp\left[-\frac{H}{R} \left(\frac{1}{T} - \frac{1}{T_0} \right) \right] - \frac{V\theta}{L} , \tag{4}$$

where H is the activation energy for healing and L is the characteristic slip distance for weakening. In isothermal condition with $T = T_0$, Equation (4) simplifies to the aging law (Ruina, 1983) that allows healing at stationary contact. An extensive body of experimental work suggests that the nucleation and initial propagation of small ruptures are governed by different mechanisms from large ones owing to the onset of lubrication at high temperature and high slip speed (Di Toro et al., 2004, 2006; Han et al., 2007; Rempel and Weaver, 2008; Di Toro et al., 2011; Kitajima et al., 2011; Brown and Fialko, 2012; Rowe et al., 2019; Pozzi et al., 2021). We only consider models with peak temperature below $\sim 1000\,^{\circ}$C, i.e., lower than the solidus of common rocks at intermediate pressure, wet conditions (Bowen, 1915; Richet and Bottinga, 1984, 1986; Navrotsky, 1995). For example, the wet solidus for granite at 100 MPa is about 900 °C (Boettcher and Wyllie, 1968) and basalt starts to melt at about 1070 °C (Hill and Boettcher, 1970). As a result, the model is only applicable to slow-slip events, tremors, small-magnitude isolated earthquakes and swarms, for which the amount of shear heating and temperature is insufficient to activate additional strong weakening mechanisms.

Under the assumptions of the physical model, given that $a > 0$ and $Q > 0$, a sudden increase of velocity and temperature, respectively, is always associated with a direct strengthening and weakening effect, respectively. However, the velocity and temperature dependence of steady-state frictional strength, given by

$$\tau_{ss} = \mu_0 \bar{\sigma} \left(\frac{V}{V_0} \right)^{\frac{a-b}{\mu_0}} \exp\left[\frac{aQ - bH}{\mu_0 R} \left(\frac{1}{T} - \frac{1}{T_0} \right) \right] , \tag{5}$$

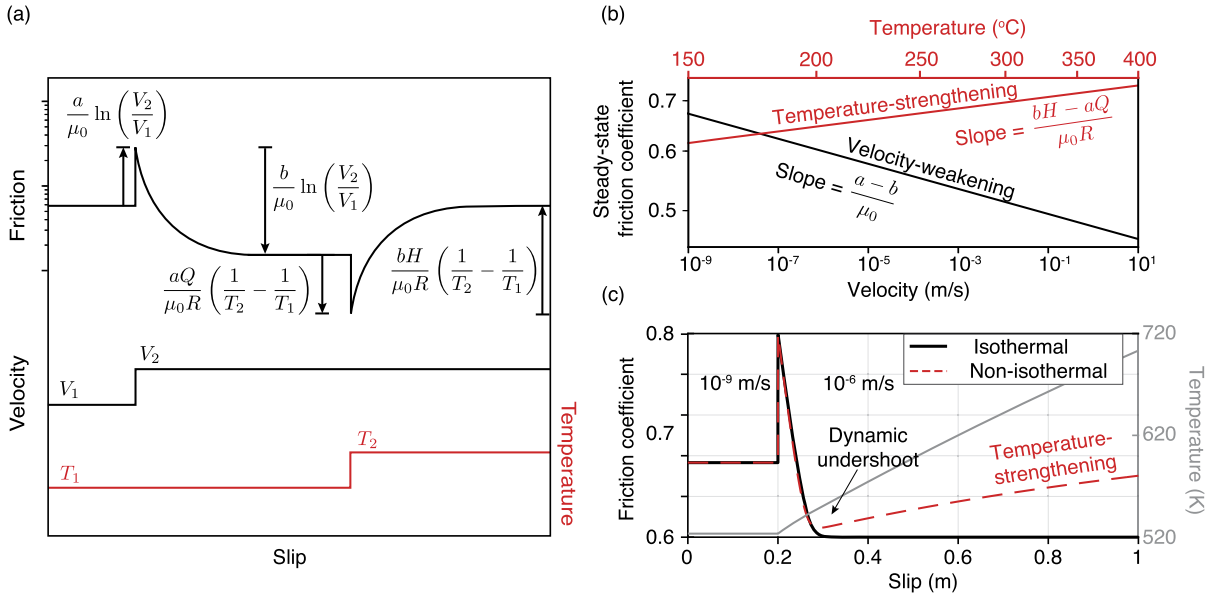

Fig. 1. Direct and steady-state rate- and temperature-dependence of frictional resistance. a) Frictional response to imposed velocity and temperature steps highlighting the direct effect and the evolutionary phase. The y-axis is logarithmic. b) Steady-state friction coefficient as a function of velocity and absolute temperature, in the case of velocity-weakening, temperature-strengthening friction, representative of the seismogenic zone. The x-axis for velocity is log-scale while the temperature x-axis is linear in $1/T$, where T is the absolute temperature. c) Evolution of the friction coefficient to a velocity step with dynamic temperature changes caused by shear heating, highlighting the dynamic undershooting caused by temperature-hardening.

can be different. Accordingly, the steady-state velocity dependence is controlled by $a-b$, with $a>b$ and $a<b$ leading to velocity-strengthening and velocity-weakening, respectively. The strength of the direct and evolutionary temperature effects are characterized by aQ and bH, respectively, with $aQ<bH$ and $aQ>bH$ leading to steady-state temperature-strengthening and temperature-weakening, respectively (Fig. 1). All combinations of velocity and temperature strengthening or weakening are possible theoretically, depending on the constitutive parameters. However, simultaneous velocity-weakening and temperature-strengthening at steady state is commonly observed in laboratory experiments (e.g., Tian and He, 2019; Liu and He, 2020; Mitchell et al., 2016; Valdez et al., 2019; An et al., 2020). For example, in the velocity-weakening range of temperatures of the seismogenic zone, granite showcases temperature-strengthening behavior (Blanpied et al., 1995). At shallow crustal conditions, natural gouge from the San Andreas Fault and the Alpine Fault exhibits velocity-strengthening, temperature-weakening at steady state (Coble et al., 2014; Valdez et al., 2019).

Equations (3) and (4) describe the fault constitutive behavior. To complete the system, we consider the conservation of energy. We assume that heat transfer results from the competition between shear heating and off-fault diffusion, neglecting the chemical reactions such as carbonate decomposition, diagenesis, and higher grades of metamorphism that may affect temperature evolution. To simplify the numerical burden, we neglect fault-parallel diffusion and adopt a membrane diffusion model, whereby the temperature follows the ordinary differential equation (Rice, 2006; Segall et al., 2010; Wang and Barbot, 2020)

$$\dot{T}=-\frac{D}{W^2}\left(T-T_{\rm b}\right)+\frac{\tau V}{w\rho c} \tag{6}$$

where $D=10^{-6}$ m^2/s is the thermal diffusivity, T_b is the bath temperature outside the fault zone, W is the characteristic width of heat diffusion, w is the width of the active slip zone, and $\rho c=3$ MPa/K is the volume heat capacity. We select the reference temperature T_0 as the steady-state temperature

$$T_{ss}=T_b+\frac{\mu_0\sigma V_l W^2}{w\rho c D}\,, \tag{7}$$

which is approximately equal to the bath temperature T_b given typical parameters. Finally, the stress interactions are described by elasticity within the radiation damping approximation (e.g., Tse and Rice, 1986; Fukuyama et al., 2002)

$$\dot{\tau}=\int_{-\infty}^{\infty}\mathbf{K}\cdot(\mathbf{V}-\mathbf{V}_L)\,{\rm d}A-\frac{G}{2V_s}\dot{V}\,, \tag{8}$$

where the first term on the right-hand side represents the elastic coupling between fault slip and stress and the second term is the radiation damping that approximates the contribution of stress change by shear waves radiating outward. Such quasi-dynamic simulations give qualitatively similar slip patterns as fully-dynamic simulations, despite quantitatively slower rupture propagation speed and slip velocity (Thomas et al., 2014).

Although many physical parameters are required to describe the thermo-mechanical system, their effect can be compounded in fewer non-dimensional parameters, following the Buckingham π theorem. In isothermal conditions, the system is controlled by 4 non-dimensional parameters (Barbot, 2019b). In particular, the Dieterich-Ruina-Rice number

$$R_u=\mathbb{W}\frac{(b-a)\bar{\sigma}}{G\,L}\,, \tag{9}$$

where $\mathbb{W}$ is the width of the velocity-weakening region, controls the importance of elastic interactions while

$$R_b=\frac{b-a}{b} \tag{10}$$

controls the importance of the evolutionary effects (e.g., Mei et al., 2021). The rupture style during seismic cycles is largely controlled by the coordinates of the physical parameters in the two-dimensional space formed by the R_u and R_b numbers (Barbot, 2019b, 2021). For example, aseismic slow-slip events occur for R_u numbers approaching unity. However, seismogenic slow-slip

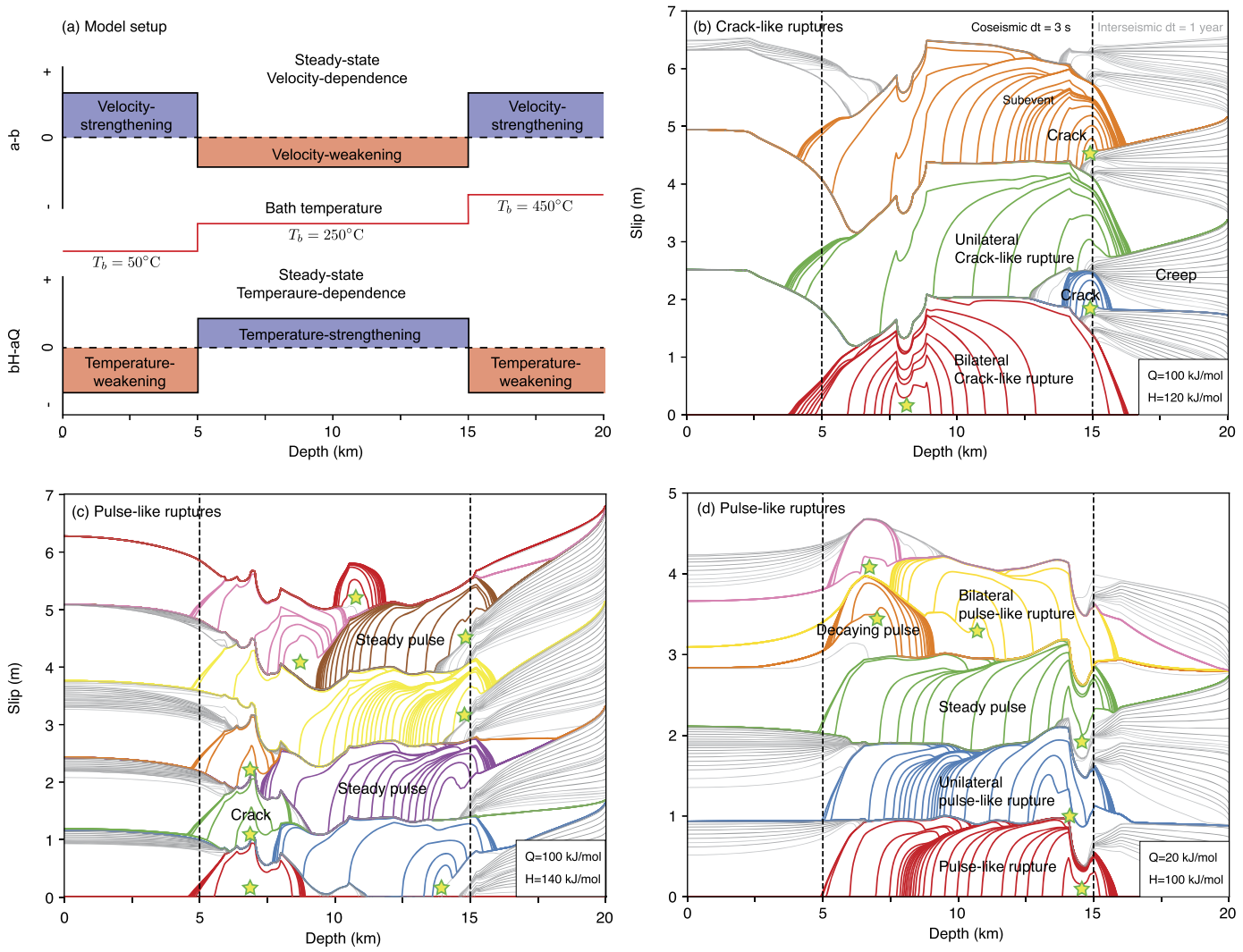

Fig. 2. a) Distribution of velocity- and temperature-dependence at steady-state along the modeled fault, and the bath temperature depth profile assumed in the model. b) Sequence of seismic events with crack-like rupture propagation with activation energies $Q = 100$ kJ/mol and $H = 120$ kJ/mol. c) Sequence combining crack-like and steady pulse-like ruptures for $Q = 100$ kJ/mol and $H = 140$ kJ/mol. d) Sequence of unilateral and bilateral pulse-like ruptures with steady and decaying pulses with $Q = 100$ kJ/mol and $H = 140$ kJ/mol. The colored isochrons feature cumulative coseismic slip every 3 seconds. The gray contours show slip isochrons every year. The yellow stars mark the hypocenters.

events, i.e., those producing low-frequency earthquakes during slow-slip propagation, occur at large R_u numbers for vanishing R_b numbers (Barbot, 2021; Nie and Barbot, 2021). For intermediate R_b numbers, large R_u numbers lead to a transition from crack-like to pulse-like rupture propagation, the emergence of aftershocks, and strong deviation from the time- and slip-predictable recurrence models (Nie and Barbot, 2022). Faults with seismogenic zones many times greater than a characteristic nucleation size typically break in seismic super-cycles (Shi et al., 2020; Barbot, 2020). In models that incorporate wave-mediated stress transfer, the R_u and R_b also numbers control the emergence of super-shear ruptures (Liang et al., 2022).

A dimensional analysis of the governing equations in non-isothermal conditions (Supplementary Materials) reveals additional non-dimensional parameters that provide additional degrees of freedom in the system (Table S1). Two parameters describe the rheological controls from the temperature dependence of friction. The Chester-Higgs number

$$R_h = \frac{bH - aQ}{RT_0} \tag{11}$$

measures the temperature dependence of steady-state friction. Steady-state temperature-strengthening and temperature-weakening corresponds to $R_h > 0$ and $R_h < 0$, respectively. The Arrhenius number

$$\alpha = \frac{bH}{RT_0} \tag{12}$$

describes the effect of activation enthalpy on fault healing. Any combination of R_h and α forms another valid non-dimensional number describing the system. For example, the non-dimensional ratio

$$R_g = \frac{bH - aQ}{bH} \tag{13}$$

provides a measure of the relative activation energies for healing and weakening. The other non-dimensional numbers depend on the characteristic time scales for different physical processes. Any ratio of the representative time scales for shear heating

$$t_s = \frac{w\rho c\, T_0}{\mu_0 \bar{\sigma}\, V_L}\,, \tag{14}$$

temperature diffusion

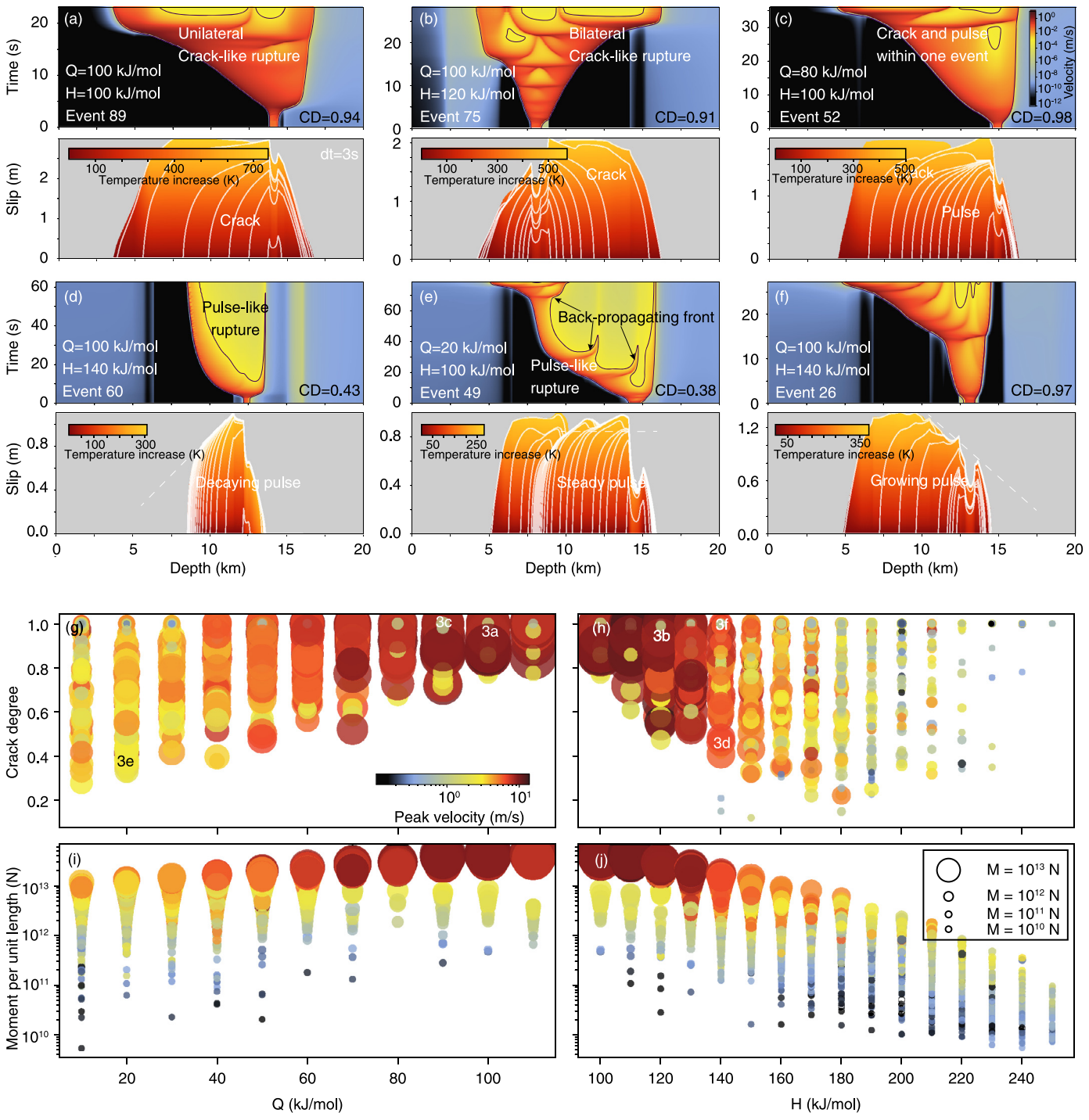

Fig. 3. Crack-like and pulse-like ruptures in seismic cycles. a-f) Individual events in seismic cycles showing different rupture styles. The subfigures from top to bottom show the history of coseismic slip velocity and the slip evolution every 3 s with the background colored by temperature. Black contour shows where slip velocity equals 1 mm/s. The crack degree (CD) is shown at the bottom right of each subfigure. g) Crack degree of all events over cycles as a function of activation energy Q. Each dot represents an event, scaled with moment and colored by peak velocity. h) Similar to (g), crack degree as a function of activation enthalpy H. i,j) Event moment as a function of Q and H, respectively.

$$t_d = \frac{W^2}{D}\,, \tag{15}$$

and evolution of the real area of contact

$$t_a = \frac{L}{V_L} \tag{16}$$

represents a non-dimensional number controlling the system. For example, the ratio

$$F = \frac{\mu_0 \bar{\sigma} L}{w \rho c T_0} \tag{17}$$

represents the relative importance of shear heating on the healing process. The dimensional analysis sheds light on how the combinations of physical parameters impact the seismic cycle and inform our numerical exploration of the parameter space.

To explore the dynamics of a steady-state velocity-weakening, temperature-strengthening asperity, we consider a 20-km long vertical fault embedded in a two-dimensional elastic domain in anti-

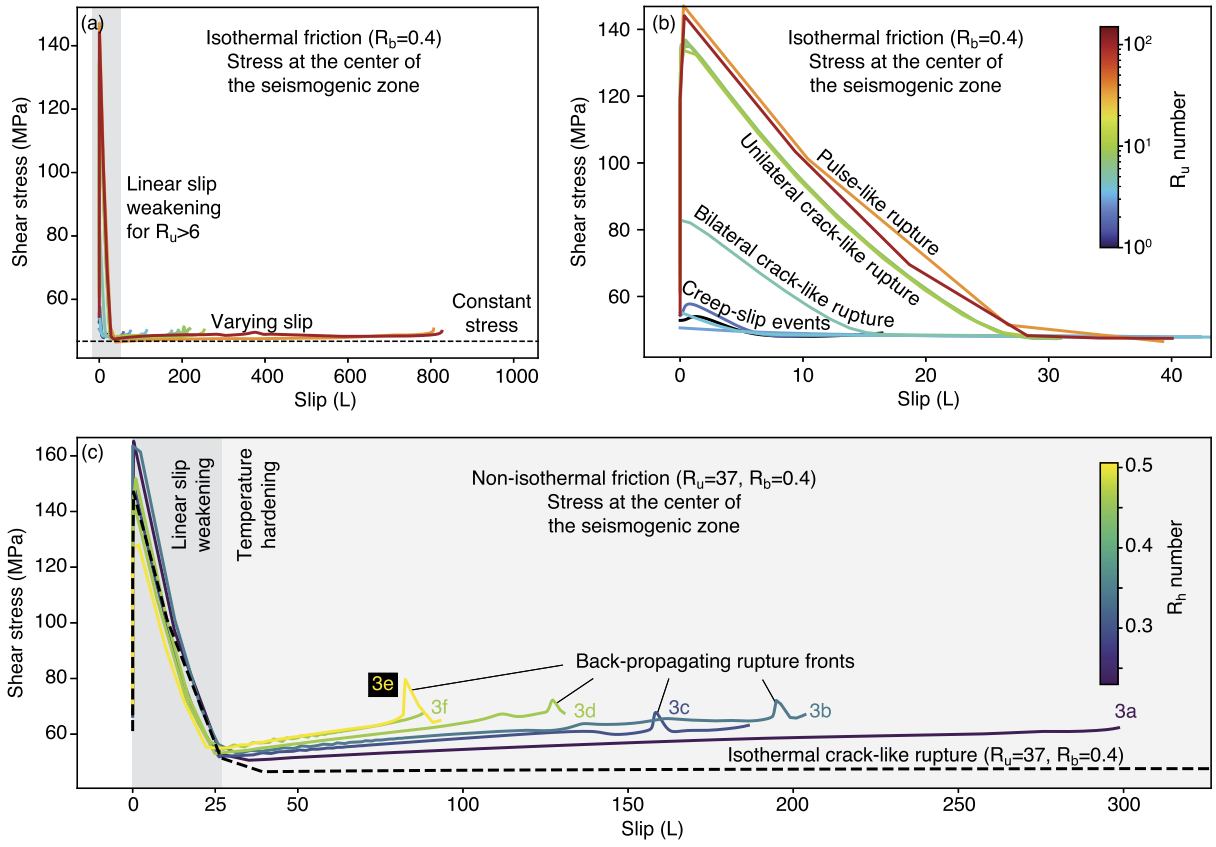

Fig. 4. Stress evolution at the center of the seismogenic zone during coseismic ruptures. a) Case of isothermal friction with varying R_u numbers assuming $R_b = 0.4$. Slip is measured in units of the characteristic weakening distance L. b) Blow-up of the gray-shaded part in (a) showing a transition to linear slip weakening with increasing R_u number (profile color). Events with $R_u < 6$ feature bilateral ruptures preceded by creep invading the seismogenic zone. c) Stress evolution with non-isothermal friction with varying R_h numbers assuming $R_u = 37$ and $R_b = 0.4$, illustrating a transition from linear slip weakening to temperature hardening for slip greater than 25 L. The event numbers refer to Fig. 3. The profiles are colored by the Chester-Higgs number $R_h = (bH - aQ)/(RT_0)$. The isothermal case (dashed line) is shown for comparison.

plane strain condition. We solve the governing equations numerically using the boundary integral method with fifth-order Runge-Kutta adaptive time steps (Barbot, 2019a). The numerical simulations benefit from extensive benchmarks limited to isothermal conditions (Erickson et al., 2020; Jiang et al., 2022). We consider constant physical parameters within the velocity-weakening region and therefore adopt stratified properties down the fault. The fault is discretized into $N = 800$ patches of size $\Delta x = 25$ m, resolving the theoretical cohesive zone width $L_b = \frac{GL}{b\sigma}$ by a factor of 4. The unstable asperity lies in the depth range 5-15 km, surrounded by two velocity-strengthening, temperature-weakening layers (Fig. 2a). Each region is associated with temperatures of 50 °C, 250 °C, and 400 °C from top to bottom, corresponding to a geotherm of 20-25 °C/km. The default parameters are shown in Table S2 with the corresponding non-dimensional numbers shown in Table S1.

3. Results

In this section, we explore the range of rupture styles and recurrence patterns that spontaneously emerge during seismic cycles in a velocity-weakening, temperature-strengthening asperity, particularly focusing on behaviors that do not occur in isothermal conditions. The range of behaviors that develops in isothermal conditions is quite varied depending on the R_u and R_b numbers, including creep, waves of partial coupling, aseismic and seismogenic slow-slip events, creep-slip events, unilateral and bilateral ruptures, full and partial ruptures, crack-like and pulse-like ruptures, with possibly foreshocks, mainshocks, and aftershocks (Barbot, 2019b; Nie and Barbot, 2021, 2022). Considering the temperature effects adds four degrees of freedom, which is challenging to explore thoroughly. To keep the problem tractable, we focus on the dynamics of a relatively unstable asperity with $R_u = 37$ and $R_b = 0.4$ that produces cycles of full and partial unilateral crack-like ruptures in isothermal conditions. We seek to identify how the rupture style differs when temperature is allowed to vary dynamically.

Other considerations reduce the dimension of the model space further. First, realistic values of thermal diffusivity of crustal rocks make heat diffusion much longer than rupture duration in most cases of interest. As a result, we can focus the parameter exploration to varying activation energies for healing and weakening and to varying widths of the active slip zone. Second, shear heating is exceedingly sensitive to the latter, and we only present numerical simulations that give rise to realistic fault temperature below 1,000 °C, essentially providing a lower bound on the width of the active shear zone.

A preliminary exploration of seismic cycles (Fig. S1) shows a wide range of different behaviors compared to isothermal friction as the activation energy for weakening decreases, the activation enthalpy for healing increases, and the width of the active slip zone decreases. In all cases, more pronounced temperature-strengthening gives rise to a transition from crack-like to pulse-like rupture propagation, transitioning further to swarms of small earthquakes and to tremorgenic slow-slip events. The width of the shear zone layer has a similar effect on seismic cycles as the activation enthalpy for healing. However, a very thin active shear zone leads to unrealistically high peak temperature. Consequently, for the rest of the study, we focus on the effects of the activation energy for healing and weakening, effectively varying the R_h and α

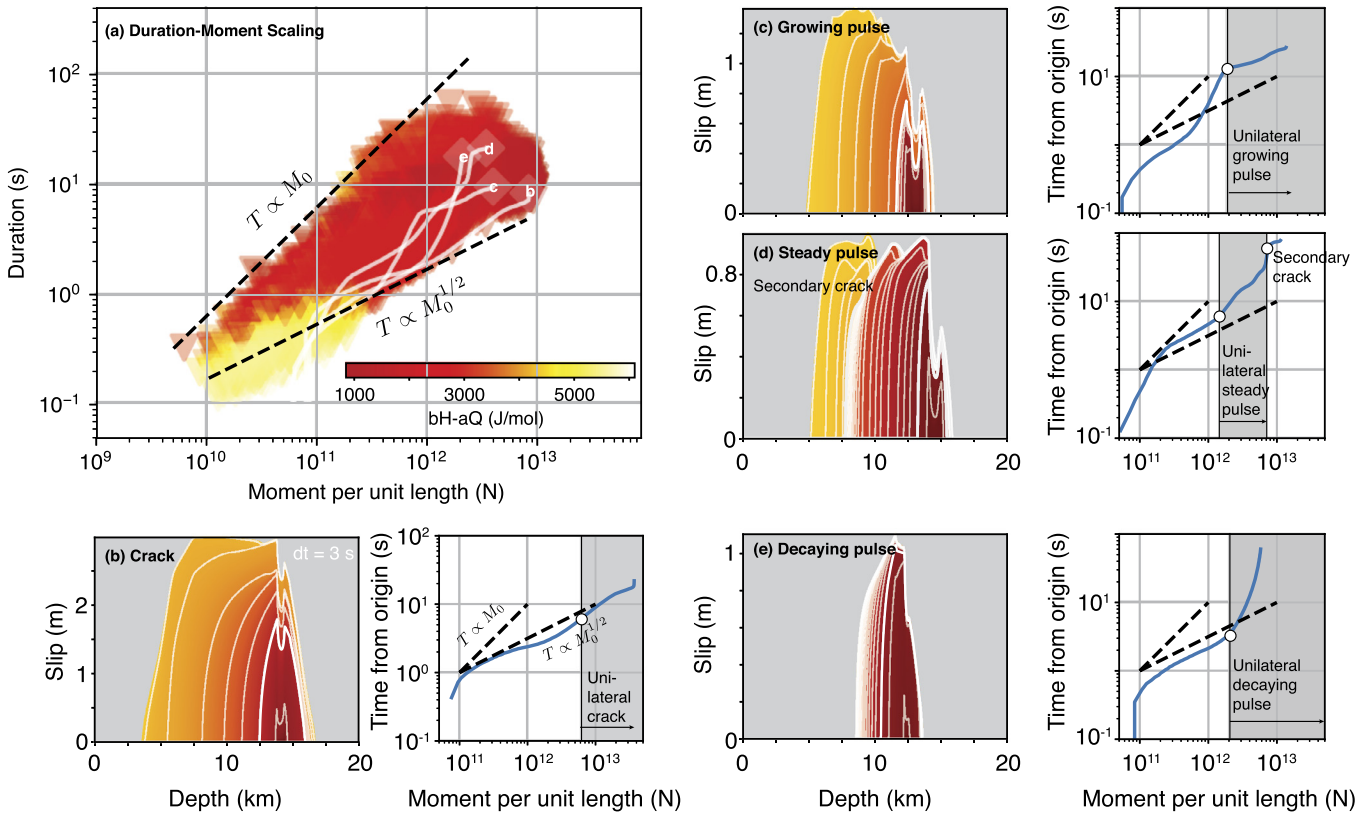

Fig. 5. Impact of rupture style on moment-duration scaling. a) Moment-duration scaling relationship for simulated fast events. Each triangle represents an event, color-coded by the input parameter $bH - aQ$. The dashed lines show the theoretical expectation for crack-like and steady pulse-like ruptures in two dimensions. The white lines show the moment-duration trajectory of the four example events with different rupture styles. b-e) Slip snapshots evolution and moment-duration trajectory of the four example events shown as diamonds in (a). The example events are the same as those in Fig. 3afed with their color indicating the time since nucleation. Gray-shaded area highlights the period when the event develops into its mature stage.

numbers defined in Equations (11) and (12), respectively, but also vary the bath temperature T_b to explore the effect of the F ratio defined in (17).

3.1. Crack-like to pulse-like ruptures

We first describe the transition from crack-like to pulse-like rupture propagation (Figs. 2 and 3). We start with a reference model with relatively high activation energies for healing and weakening ($Q = 100$ kJ/mol, $H = 120$ kJ/mol) giving rise to sequences of seismic events with crack-like rupture propagation. The isochrons reveal the occurrence of slip during virtually the entire rupture duration, with either unilateral or bilateral rupture propagation. Increasing the activation enthalpy for healing ($H = 140$ kJ/mol) creates sequences with more frequent partial ruptures of lower stress drop, shorter recurrence times, and with the larger ruptures propagating unilaterally as steady pulses. In the case of a reduced activation energy for the direct effect of temperature ($Q = 20$ kJ/mol), the large ruptures showcase bilateral and unilateral ruptures propagating as steady pulses.

For more gradual changes of physical parameters and many subsequent ruptures in a continuous sequence, a wide range of rupture sizes with infinitely varying details of rupture propagation can be found. Careful examination of a large number of ruptures for a wide range of physical parameters reveals different types of rupture propagation. Fig. 3d-f shows examples of decaying, steady, and growing pulses, respectively. These types of pulses were reported in single event simulations with strong weakening at high velocity where the initial conditions can be specifically tuned (e.g., Zheng and Rice, 2009; Noda et al., 2009; Gabriel et al., 2012). In seismic cycle simulations, some pulse-like ruptures are observed (e.g., Idini and Ampuero, 2020; Heimisson, 2020; Lambert et al., 2021), but this is the first time, to our knowledge, that all three types of pulse-like ruptures are documented.

To capture the bulk of this variability, we define the crack degree of any single rupture as the ratio of the area of high slip rate (greater than 1 mm/s) over the total rupture area in time and space (Fig. 3a-f; see Supplementary Materials for more details). The crack degree, peak velocity, and moment magnitude of seismic events vary systematically with activation energy (Fig. 3g-j), indicating the gradual transition from crack-like to pulse-like rupture with increasing temperature-strengthening. However, not all events in any cycle propagate as a pulse, even in cases where the thermal effect is most pronounced (Fig. 2c). It is the crack degree of the most pulse-like event that decreases with enhanced temperature effect. Furthermore, some events feature both crack-like and pulse-like rupture propagation (Fig. 3c), as crack-like sub-events can initiate near the end of the previous pulse-like ruptures.

In seismic cycles simulations assuming isothermal friction, pulse-like rupture propagation may occur at high R_u number due to the emergence of stress concentrations left by previous partial ruptures (Nie and Barbot, 2022). For sufficiently high R_u numbers, the stress follows a linear slip weakening profile, whereby slip greater than about 25 times the characteristic weakening distance — often referred to as D_c — occurs at low, virtually constant stress (Fig. 4a,b). Assuming non-isothermal friction, a transition occurs from linear slip weakening to temperature hardening with accrued slip (Fig. 4c). The amount of temperature hardening is controlled by the Chester-Higgs number. Temperature hardening caused by shear heating enables a transition from crack-like to pulse-like rupture propagation with rapid healing behind the rupture front (see Fig. 1c, 4c). The rapid fault restrengthening locks the asperity

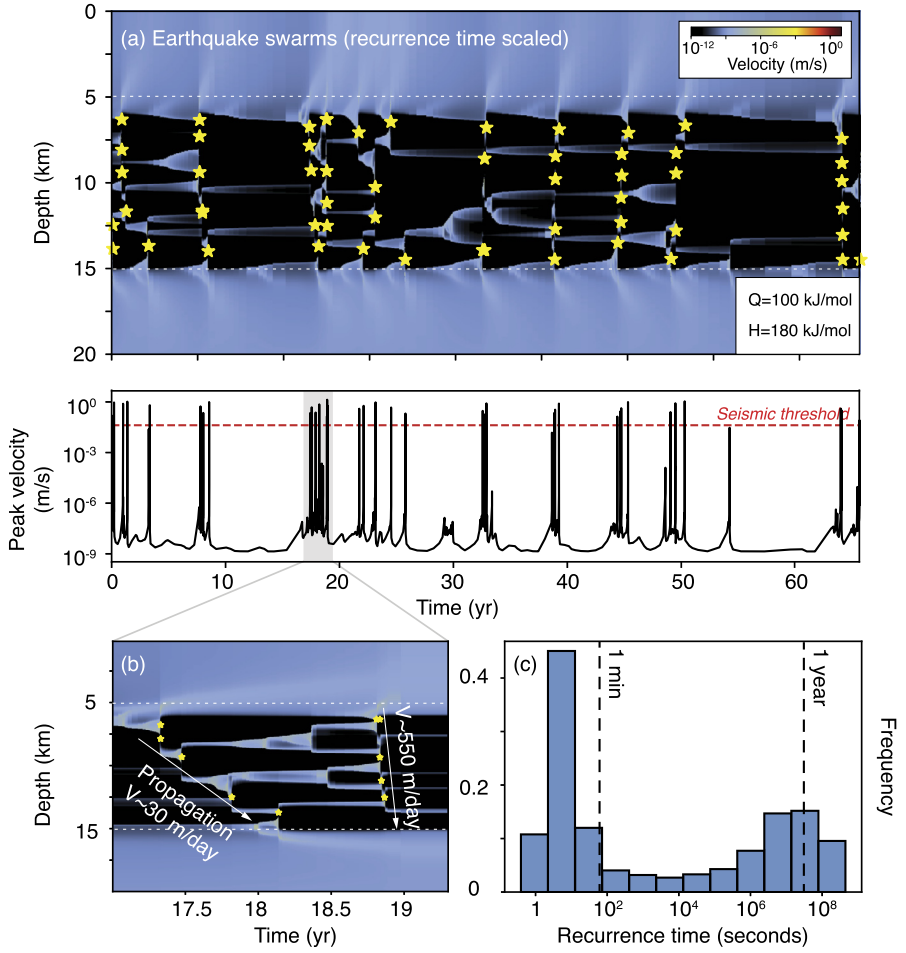

Fig. 6. Earthquake swarms in a simulation with $Q = 100$ kJ/mol and $H = 180$ kJ/mol ($R_h = 0.69$). The recurrence time is tuned (see Fig. 7(a)) to be several years by using $L = 2.5$ mm, $\sigma = 25$ MPa, and $w = 5$ mm. a) Spatio-temporal evolution of slip velocity on the fault. The white dashed lines mark the boundary of the velocity-weakening, temperature-strengthening region. The yellow stars mark the hypocenters of earthquakes. The subfigure below shows the peak slip velocity time series. The red dashed line indicates the velocity threshold above which the radiation pattern dominates and an event is considered seismic. The gray shaded patch marks the time range shown in (b). b) Zoomed-in view of the spatio-temporal evolution of slip velocity highlighting the propagation of swarms. c) Distribution of inter-event time. The distribution is bimodal, characteristics of seismic swarms.

before rupture arrest, giving rise to a propagating pulse. The same effect reduces the final stress drop and the peak velocity, every other parameters being the same. As a result, the recurrence time of earthquakes, stress drop, peak velocity, and moment magnitude all vary as a function of the thermodynamic properties.

3.2. Moment-duration scaling of crack-like and pulse-like ruptures

The spontaneous occurrence of ruptures with crack-like and pulse-like propagation in our simulations sheds new light on the moment-duration scaling of natural earthquakes. The moment-duration relationship of slow and fast earthquakes reflects the mechanics of rupture propagation. Regular fast earthquakes typically follow a cubic moment-duration scaling with $M_0 \propto t_r^3$, where M_0 is the seismic moment and t_r is the rupture duration, for a wide range of magnitudes (Kanamori and Anderson, 1975; Houston, 2001), consistent with a self-similar circular crack expanding at a constant stress drop. However, the observations show some scatter (Wells and Coppersmith, 1994; Allmann and Shearer, 2009; Peng and Gomberg, 2010) that is attributed either to the natural variability of static stress drop, or to structural boundaries creating elongated ruptures (Hanks and Bakun, 2002; Gomberg et al., 2016). A deviation from the cubic moment-duration scaling for large megathrust earthquakes is also reported in recent studies (Meier et al., 2017).

We suggest that the pulse-like or crack-like character of rupture propagation also contributes to this complexity. Ruptures with crack-like and pulse-like propagation style follow different moment-duration scaling relationships. The average slip increases with rupture length for crack-like ruptures, implying $M_0(t) \propto t^3$ for finite-size faults where t is the time since the start of the event and $M_0(t)$ is the moment released till time t. Notice the difference between time t and duration t_r. In contrast, slip remains constant during steady pulses, implying $M_0(t) \propto t^2$. We illustrate this relationship within the two-dimensional approximation of our models that gives rise to $M_0 \propto t_r^2$ and $M_0 \propto t_r^1$ for crack-like and pulse-like ruptures, respectively (Fig. 5). The simulated events fall within the above theoretical predictions. All the events are bounded by two straight lines corresponding to the crack- and steady pulse-like rupture end-members. However, the moment-duration trajectory formed by the time-dependent coordinates $M_0(t), t_r(t)$ of individual events, where t is the time since nucleation, shows some complexity (e.g., Fig. 5b-e), as different processes unfold within the span of a single rupture. After the nucleation phase, transitions from bi-lateral to uni-lateral or from crack-like to pulse-like propagation can occur, affecting the moment rate. As the rupture continues, the details of rupture propagation alter the final moment and duration of the rupture, explaining the natural scatter.

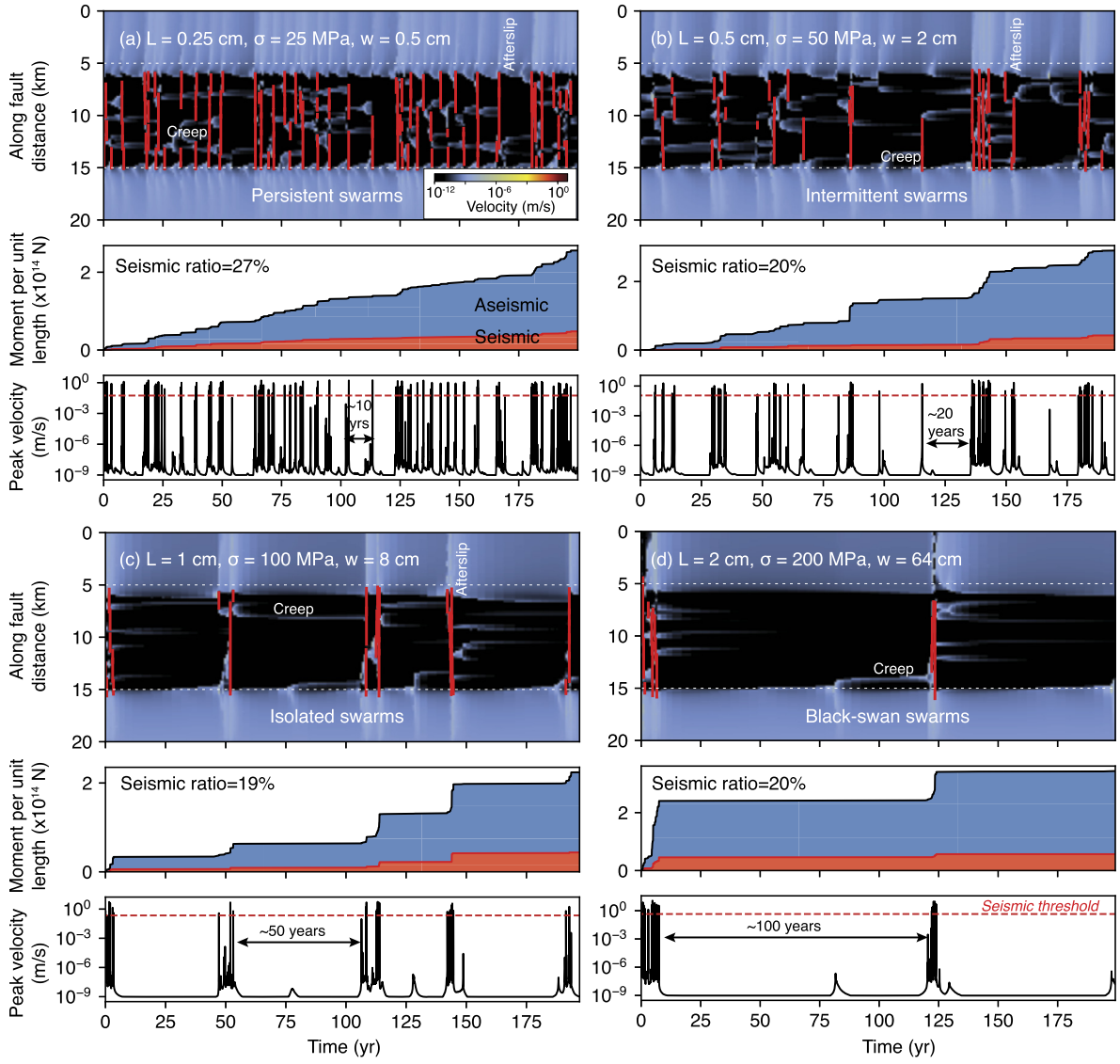

Fig. 7. Simulations for varying characteristic weakening distance L, effective normal stress $\bar{\sigma}$ and width of the active shear zone w with fixed non-dimensional numbers, producing swarms with varying recurrence timescales. Each simulation shows the spatio-temporal evolution of slip velocity on the fault, the cumulative moment release history, and the peak velocity time series. We change the parameters to keep all non-dimensional numbers constant: $L' = kL, \sigma' = k\sigma, w' = k^2 w$, with k a real number between 1 and 8.

3.3. Seismic swarms

As the temperature-strengthening effect increases, corresponding to larger R_h, the seismic cycles feature clusters of small events spanning the width of the seismogenic zone (Fig. 6). We describe an example for $Q = 100$ kJ/mol and $H = 180$ kJ/mol, i.e., $R_h = 0.69$, corresponding to a higher activation enthalpy for healing compared to our reference model. The cycle lacks any large earthquake that would characterize a mainshock/aftershock sequence. Instead, the recurrence time shows a bimodal distribution with peaks varying by five orders of magnitude, characteristic of seismic swarms. The complete rupture of the seismogenic zone occurs in a series of partial ruptures propagating between 30 and 550 m/day.

In our models, the seismic swarms release a seismic moment between 19 and 27% of the total moment (Fig. 7), suggesting a strong interplay between fast and slow slip. The size of individual ruptures is limited by a strong temperature-strengthening effect once the rupture reaches seismic speed, continuing the trend shown in Fig. 3i,j. The rapid triggering of the following ruptures is facilitated by aseismic slip occurring as afterslip of the previous rupture. Aseismic slip within the seismogenic zone also drives the nucleation of the subsequent swarms in the next cycle.

Similar rupture propagation styles and recurrence patterns characteristic of seismic swarms can be obtained for a wide range of recurrence times by varying the effective normal stress (Fig. 7). Maintaining similar rupture dynamics as we change the effective normal stress requires keeping the R_u number and F ratio described in Section 2 constant. Any factor k applied on the effective normal stress must be compensated for by the same factor on the characteristic weakening distance (Equation (9)) and by a factor k^2 on the width of the active shear zone (Equation (17)). Using the effective normal stress $\bar{\sigma} = 25$ MPa, $L = 0.25$ cm, and $w = 0.5$ cm, we obtain persistent swarms with inter-swarm periods of the order of just 10 yr. With twice the effective normal stress, i.e., with $\bar{\sigma} = 50$ MPa, $L = 0.5$ cm, and $w = 2$ cm, the swarms become intermittent, with an inter-swarm period of 20 yr. Quadrupling the effective normal stress to $\bar{\sigma} = 100$ MPa, and compensating with $L = 1$ cm and $w = 8$ cm, we obtain isolated swarms emerging after about 50 yr of apparent quiescence. Octupling the effective nor-

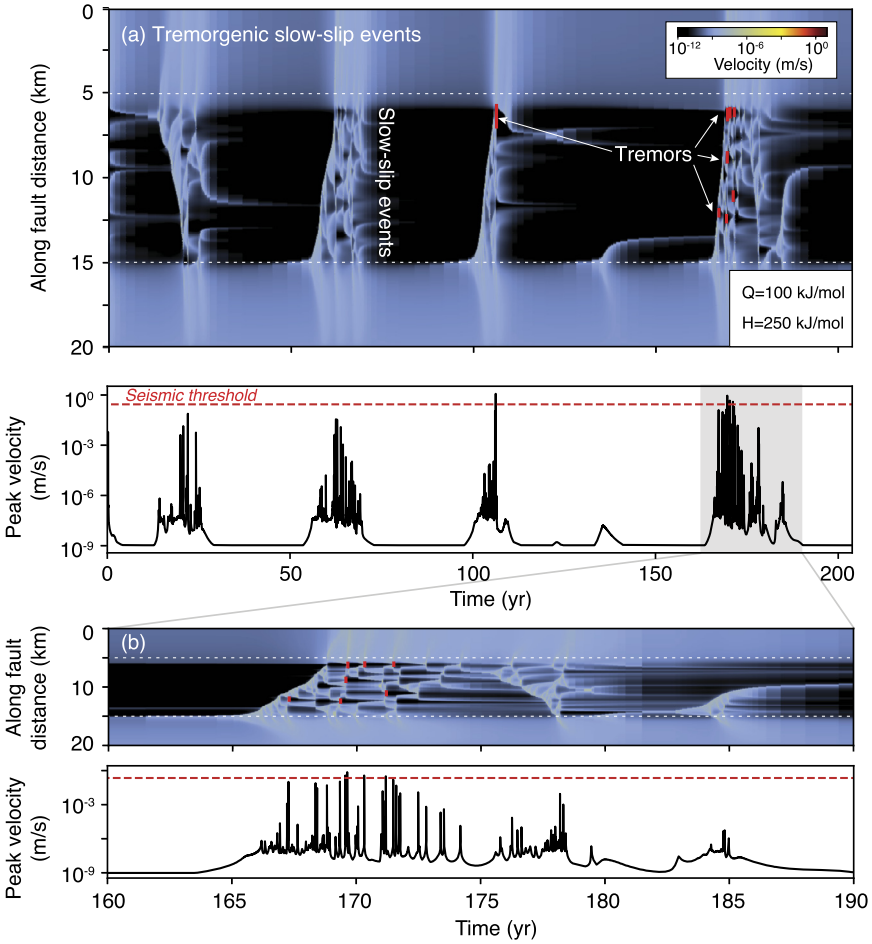

Fig. 8. Nested tremorgenic slow-slip events in simulations with $Q = 100$ kJ/mol and $H = 250$ kJ/mol ($R_h = 1.1$). a) Spatiotemporal evolution of slip velocity on the fault. The white dashed lines mark the boundary of the velocity-weakening, temperature-strengthening region. The red vertical bars represent the rupture area of tremors. The subfigure below shows peak slip velocity time series. The red dashed line indicates the velocity threshold above which the radiation pattern dominates and an event is considered seismic. The gray shaded patch marks the time range of the zoom-in vision in (b). b) Same results shown for a 30-year period.

mal stress to $\bar{\sigma} = 200$ MPa, and compensating with $L = 2$ cm and $w = 64$ cm, we obtain black-swan swarms that burst clusters of seismic events after about 100 yr of inactivity. These models may be useful to understand seismic unrest without apparent triggering and the large variation in the duration of seismic swarms (Ross and Cochran, 2021).

3.4. Tremorgenic slow-slip events

We now describe the end-member behavior corresponding to a strong temperature-strengthening effect. As a first example, we consider the case with $Q = 100$ kJ/mol and $H = 250$ kJ/mol, i.e., $R_h = 1.1$ (Fig. 8). The cycle consists of decades-long sequences of multiple bursts of slow-slip events interspersed with high-velocity ruptures, some of which attaining seismic speed. Although the dominant mode of rupture is aseismic, representing 98% of the total moment release, the sequence is charged with numerous small low-frequency earthquakes that we interpret as tremor activity. The temperature-strengthening constitutive behavior coupled with shear heating allows tremor-like signals to appear within a single, homogeneous asperity. Due to the complexity of fault dynamics mixing slow and fast ruptures, the recurrence patterns and slow-slip duration vary greatly.

In this particular simulation, the decades-long bursts of episodic tremor and slip are preceded by a long period of quiescence. Within each burst of episodic tremor and slow slip, there are spikes of fast and slow events propagating and re-rupturing the same asperity. The non-stationary behavior of fault dynamics — capable of generating slow-slip and tremors for decades and then locking for an indefinite period — provides a potential explanation for the lack of slow-slip events observations at some subduction zones. If the model is applicable, the subduction zones without apparent slow-slip activity may be in the locked stage of the slow-slip cycle while others currently undergo the active stage.

Similar to seismic swarms, the recurrence time between bursts of tremorgenic slow-slip events is controlled by the effective normal stress. As a result, more persistent tremorgenic slow-slip events are also possible within the physical assumptions (Fig. 9). Consider the case of an effective normal stress of $\bar{\sigma} = 20$ MPa, with $L = 2$ mm and $w = 3.2$ mm. The fault is never fully locked as creep pervades the seismogenic zone. Long tremorgenic slow-slip events lasting 6 months to a year occur with a recurrence time between 1 and 2.5 yr. With an effective normal stress of $\bar{\sigma} = 10$ MPa, $L = 1$ mm and $w = 0.8$ mm, the recurrence pattern is similar, but the frequency of seismic events within a slow-slip episode increases. With $\bar{\sigma} = 6.7$ MPa, $L = 0.67$ mm, and $w = 0.36$ mm, the duration or tremorgenic slow-slip events reduces to a few months, with inter-event times shorter than a year. At the end of the spectrum, with $\bar{\sigma} = 3.3$ MPa, $L = 0.33$ mm, and $w = 0.09$ mm, the generation of low-frequency earthquakes is sustained, only modulated by periods of more or less intense seismic activity. In all these models, the seismic moment varies between 4% and 28% of the total moment release, indicating the dominance of aseismic slip with varying amounts of tremor activity.

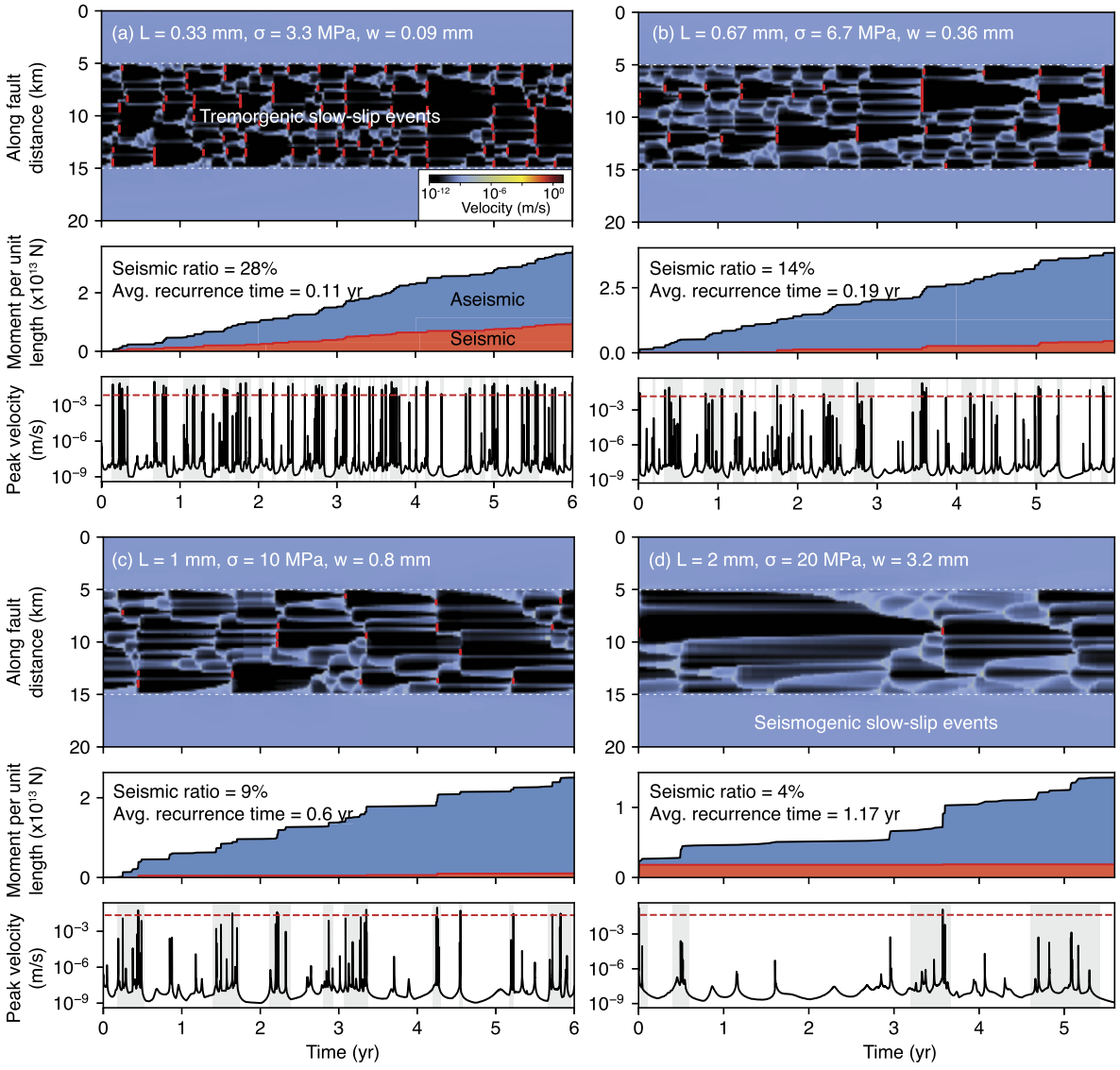

Fig. 9. Slow-slip events with different recurrence time. Simulations for varying L, σ and w with fixed non-dimensional numbers, producing tremorgenic slow-slip events with varying recurrence timescales. Each simulation shows the spatiotemporal evolution of slip velocity on the fault, cumulative moment release history and peak velocity time series. We change the parameters in a way that keeps all non-dimensional numbers constant: $L' = kL, \sigma' = k\sigma, w' = k^2 w$, with k a real number between 1 and 8.

Capitalizing on previous studies of the slow-slip phenomenon in isothermal conditions, we summarize the diverse range of slow-slip behaviors allowed by rate-, state-, and temperature-dependent friction within a homogeneous velocity-weakening, temperature-strengthening asperity (Fig. 10). The temperature-strengthening effect allows the generation of tremors at high R_u numbers. While different effective normal stresses produce sequences with intermittent to persistent tremors, changing the R_u number produces a range of slow-slip events with varying seismic contribution, possibly characterized as tremorgenic with $R_u = 37$, seismogenic with $R_u = 16$, transitioning to periodic seismogenic with $R_u = 4$ and completely aseismic with $R_u = 2$. We conclude that a wide range of parameters can produce aseismic, seismogenic, and tremorgenic slow-slip events when thermally activated friction is taken into consideration.

3.5. Role of the Chester-Higgs number

We complete the parametric study by determining the non-dimensional number that controls the change of rupture style. Exploration of thermodynamic parameters within the range $10 \leq Q \leq 110$ kJ/mol and $100 \leq H \leq 250$ kJ/mol indicates a systematic evolution of the maximum moment per unit length, the minimum crack degree, the peak slip velocity, and the seismic moment ratio, all diagnostic aggregate features to identify rupture style (Fig. 11).

The competition between direct thermal weakening and time-dependent thermal strengthening is captured by the Chester-Higgs number R_h (Equation (11)). The boundaries between different rupture dynamics are sub-parallel to the R_h contours. Regardless of the combination of the activation energies Q and H, crack-like rupture propagation occurs for $R_h \leq 0.4$; pulse-like rupture propagation occurs in the range $0.4 \leq R_h \leq 0.65$; seismic swarms fall in the range $0.65 \leq R_h \leq 1$, and tremorgenic slow-slip events occur for $R_h \geq 1$. This indicates that a single non-dimensional parameter captures the main temperature control of seismic cycles in the H-Q two-dimensional space within the assumptions of the model.

The primary control on fault dynamics by the Chester-Higgs number R_h is further confirmed by looking at the phase diagram in non-dimensional number space (Fig. 11, S3, S4). The diagnostic aggregate features and overall fault slip patterns do not vary much at different Arrhenius number α (Equation (12)) with the same R_h number (Figs. 11 and S3), but weakly modulated by the

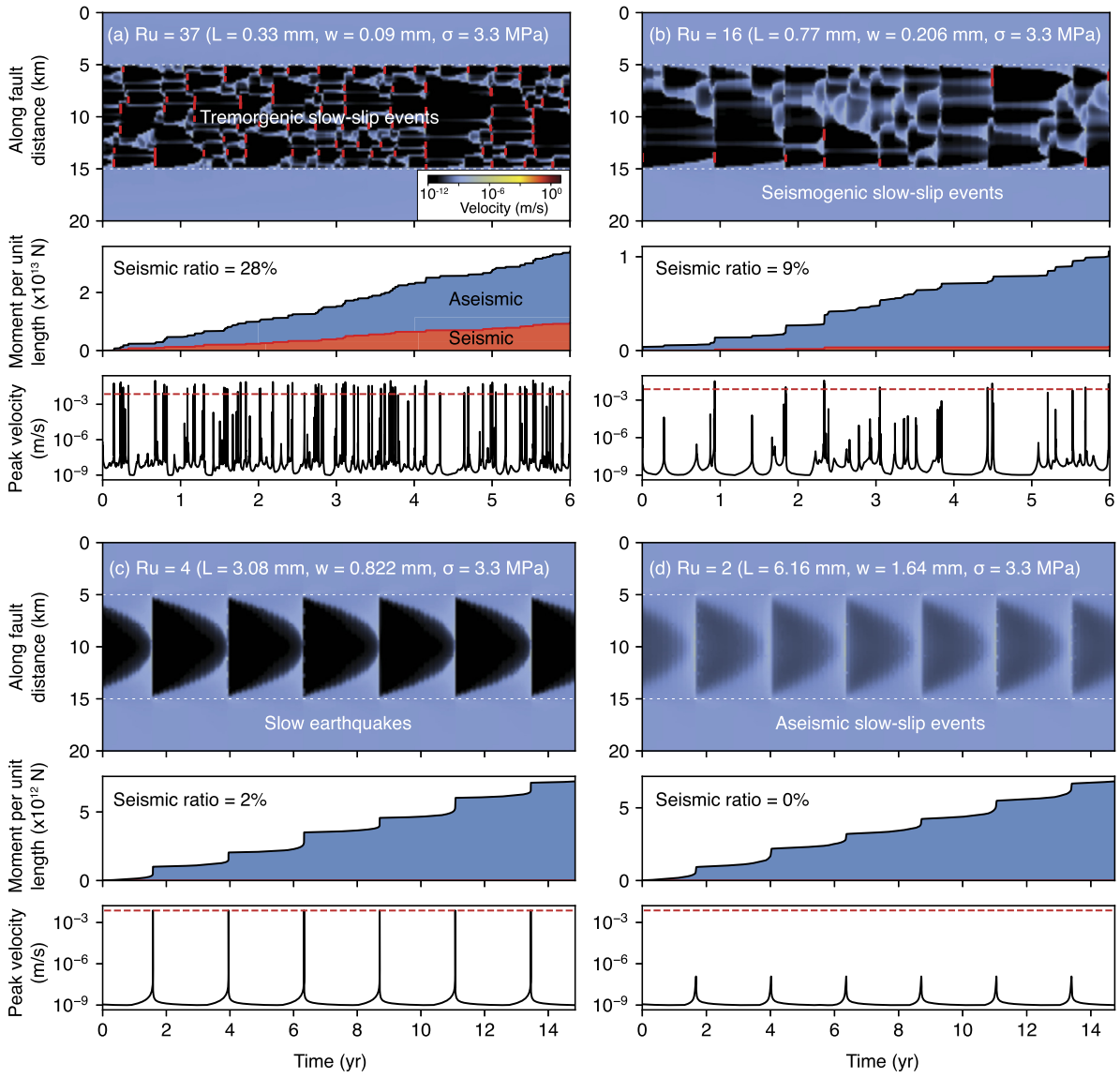

Fig. 10. Simulated slow-slip events over a wide range of R_u. Each simulation shows the spatio-temporal evolution of slip velocity on the fault, cumulative moment release history and peak velocity time series. To simulate a subduction environment, the model setup assumes a uniform background temperature of 250 °C with a temperature-strengthening fault.

F ratio (Equation (17), Figs. S1 and S4). We conclude that the temperature-related effects on seismic cycles are primarily controlled by the Chester-Higgs number R_h.

4. Discussion

The variety of the seismic phenomenon originates in part from the complexity of the thermo-mechanics of deformation at the micro-scale within the fault zone. Our study delineates important end-member rupture styles that do not spontaneously occur in isothermal conditions. The coupling between steady-state temperature-strengthening and shear heating during seismic ruptures provides a mechanism for rapid relocking behind the rupture front that favors a pulse-like propagation. As a consequence of lateral variations of initial stress before any rupture during seismic cycles, steady, growing, and decaying pulses can occur spontaneously. With increasingly dominant temperature-strengthening effects, seismic swarms and tremorgenic slow-slip events can be obtained. Considering the admissible range of physical parameters in isothermal and non-isothermal conditions, the constitutive framework may readily explain many different types of frictional instabilities observed in nature even without invoking lateral variations of frictional properties in the velocity-weakening region. A remaining question is what constitutes realistic parameters given a tectonic setting.

Experimental investigations of the thermal activation of fault friction was pioneered by Higgs (1981), Chester and Higgs (1992), and Chester (1994) on quartz-rich gouge. In dry conditions, the activation energy for the direct effect of temperature and for healing varies in the ranges $Q = 87 - 154$ kJ/mol and $H = 43 - 168$ kJ/mol, respectively. In wet conditions, the range is narrower, with $Q = 68.1 - 101$ kJ/mol and $H = 62.7 - 143$ kJ/mol. These observations are compatible with the range of activation energy $Q = 30 - 130$ kJ/mol for subcritical crack growth for various rock types (Atkinson, 1984). However, experiments on SAFOD samples from the central deforming zone, which is velocity-strengthening and temperature-weakening at steady state, show activation energy for the direct effect of $Q = 215$ kJ/mol (Coble et al., 2014). The range of activation energy for the healing process is compatible with the various microphysical healing mechanisms within the

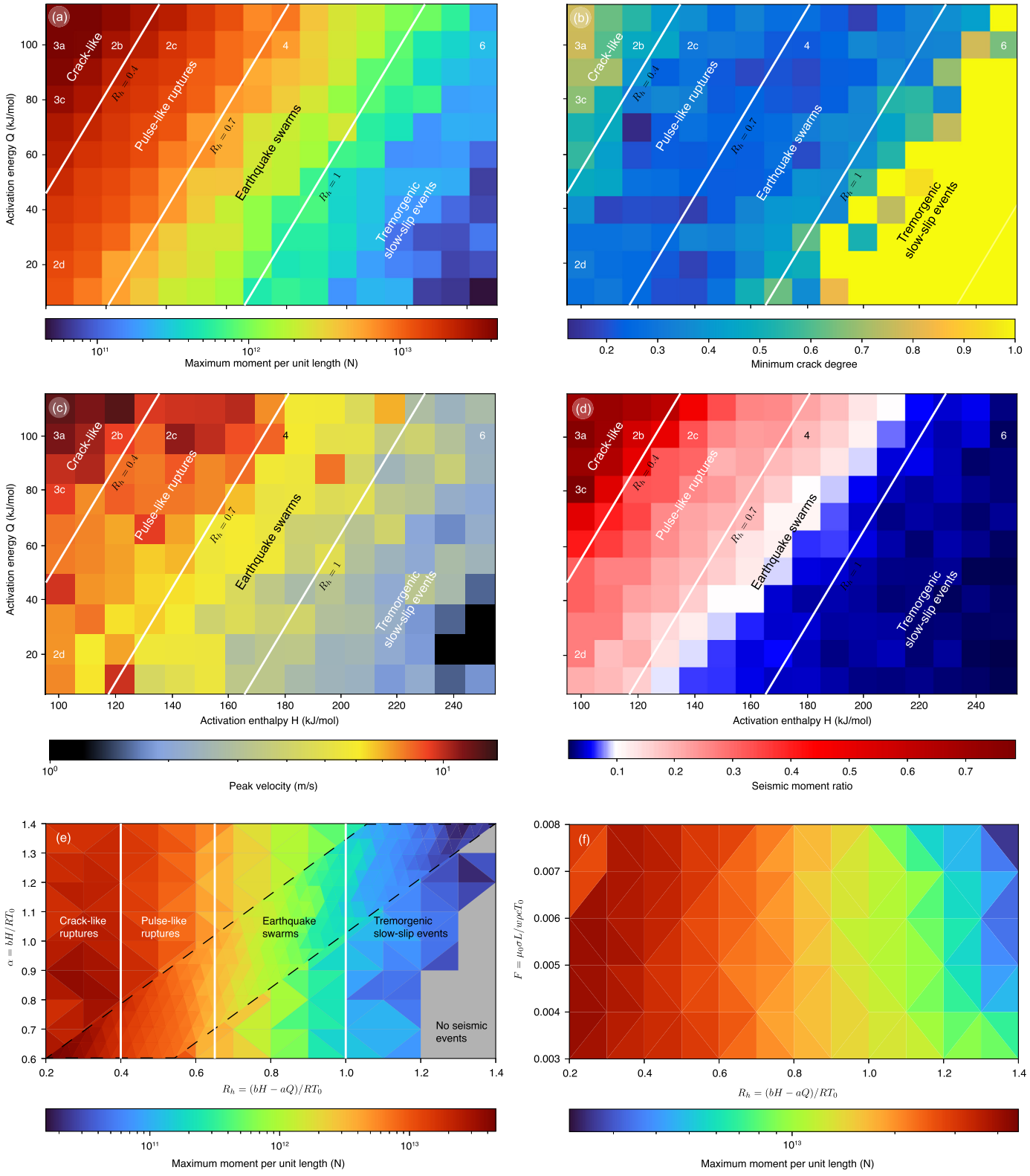

Fig. 11. Phase diagram of fault slip behavior. a-d) Phase diagram in (H, Q) space. a) Maximum moment per unit length in each simulation. b) Minimum crack degree. c) Maximum velocity. d) Seismic moment ratio. The solid white lines are R_h contours that separate domains of different rupture behaviors. Different behaviors as well as examples in previous figures are marked on the diagram. e,f) Phase diagram of the maximum moment per unit length as a function of e) the Chester-Higgs number R_h and the Arrhenius number α and f) the Chester-Higgs number R_h and the non-dimensional number F. The black dashed lines represent simulations that finely vary the activation energies H and Q in a-d). The phases diagram indicates the weak influence of the other non-dimensional parameters α and F on the rupture style. See the supplementary materials for phase diagrams of the other aggregate features (e.g., minimum crack degree).

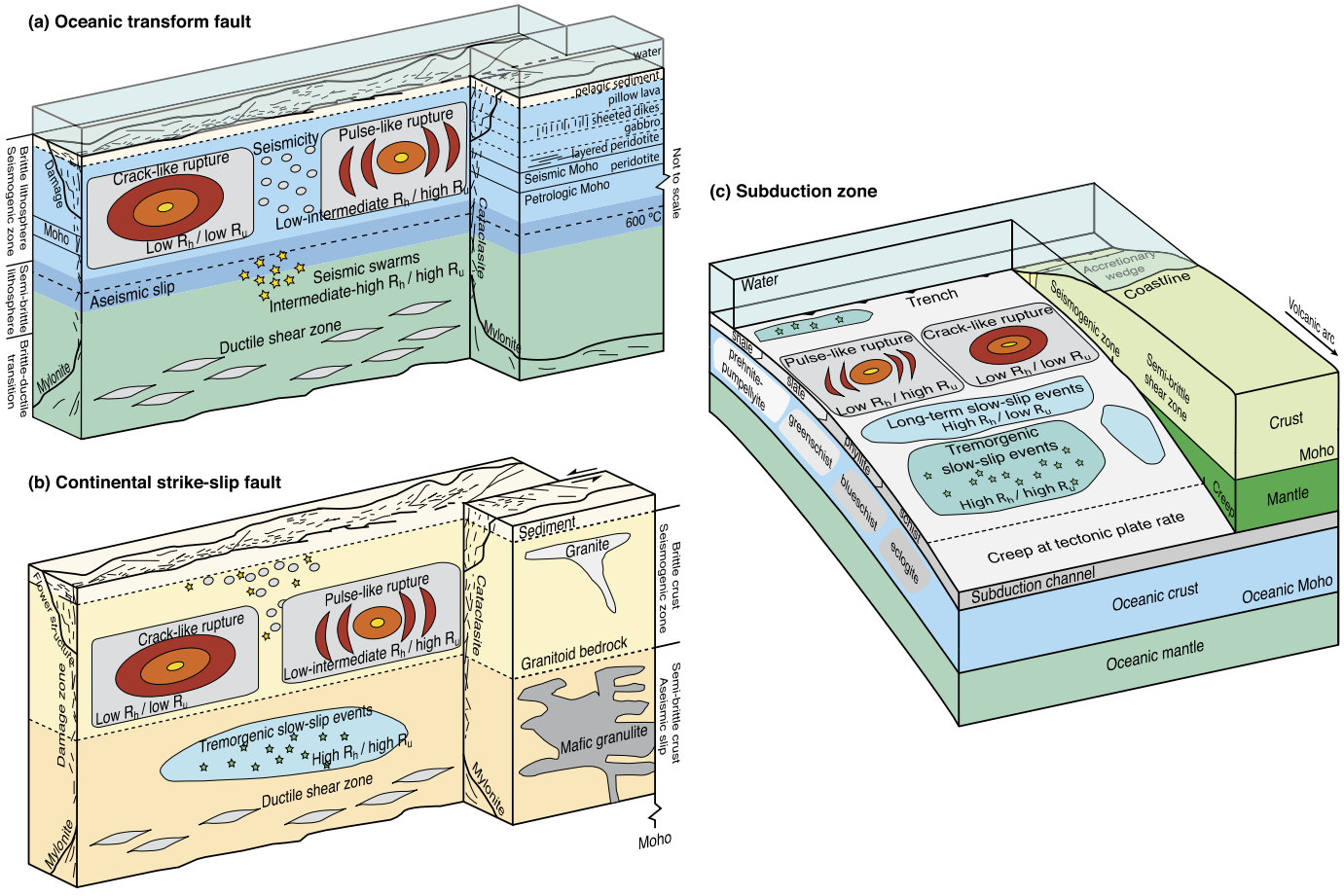

Fig. 12. Schematic of fault slip behavior in relation to the tectonic setting, mineralogy, and degree of metamorphism for a) oceanic transform faults (Kuna et al., 2019; Kohli et al., 2021), b) continental strike-slip faults (Hawkesworth and Kemp, 2006a,b; Wang and Barbot, 2020), and c) subduction zones (Shi et al., 2020; Barbot, 2020). The rock type, ambient temperature, and texture of fault zones may be captured with various non-dimensional numbers, controlling the different styles of ruptures (crack-like and pulse-like rupture propagation, seismic swarm recurrence patterns, and tremorgenic slow-slip events).

fault core, including 20-50 kJ/mol for pressure solution creep (Rimstidt and Barnes, 1980), 35-80 kJ/mol for diffusional crack healing (Brantley et al., 1990), and 30-700 kJ/mol for viscoelastic collapse (Kirby and Kronenberg, 1987; Mares and Kronenberg, 1993; Holyoke et al., 2013). Assuming that the mechanics of contact evolution at the micro-scale is rate-limited by viscoelastic processes, the range of activation energies is also compatible with 51 ± 9 kJ/mol for biotite (Kronenberg et al., 1990), 150-600 kJ/mol for feldspar (Rybacki and Dresen, 2000), and 135-240 kJ/mol for quartz (Rutter and Brodie, 2004a,b; Hirth et al., 2001), which are the main constituents of granite. The constitutive parameters used in the current study are well within the range of laboratory observations (Barbot, 2022) and make the model potentially applicable to a wide range of depths and rock types.

We suggest that the wide spectrum of fault slip observed in various tectonic settings may be associated with different activation energies for healing and weakening resulting from different protoliths, degrees of metamorphism, and micro-scale deformation mechanisms within the fault zone (Fig. 12). The structure of oceanic transforms connecting spreading centers split the oceanic lithosphere through different crustal and upper-mantle rocks, following an ophiolite sequence. Fluids reacting with fault rocks create deposits of serpentinite in peridotite mylonitic shear zones that may introduce additional structural complexity. Continental strike-slip faults also exhibit structural maturation with depth from the superficial damaged flower structure to the cataclasite of the seismogenic zone, and the deeper mylonitic shear zones. The subduction channel of subduction zones incorporates fragments of the oceanic crust and inherits pelagic and continental sediment that undergo prograde metamorphic reactions from slate, to phyllite, to schist as they travel from the deformation front to the mantle wedge corner. As the altered basalt of the subducting slab metamorphoses from greenshist, to blueschist, and then eclogite, changes of mineralogy and fault-zone texture do occur. The unique distribution of metamorphic facies at these various different tectonic settings should be reflected by different constitutive frictional properties, including activation energies.

For example, the dominant microphysical mechanisms of shear zone deformation at the high temperatures found in the deep tremorgenic zone of subduction zones down-dip the seismogenic zone are those with high activation enthalpy, such as viscoelastic flow, grain growth, or dynamic recrystallization (Platt et al., 2018). In addition, the plastic deformation of fault gouge that would require high temperature in a dry environment may nevertheless occur in the cold regime of the mid- and lower-crust due to the presence of high-pressure fluids. As the fugacity of water is thermally activated, the activation energy in wet conditions is substantially lower than in dry conditions (Karato and Jung, 2003). As a result, the prevailing deformation mechanism for tremorgenic slow-slip events may be low-temperature, wet plasticity, compatible with the high range of activation enthalpy associated with this rupture style in our models. More experimental studies should be conducted on serpentinite and other slow-slip-hosting rocks to better document their thermodynamic properties (e.g., Takahashi et al., 2011). For example, serpentinite is velocity-weakening, temperature-strengthening between 450 °C

and 600 °C (Okazaki and Katayama, 2015) at the typical depths of slow-slip and tremors (Condit et al., 2020). Seismic swarms often occur in hydrothermal regions (Mogi, 1963; Sykes, 1970; Benoit and McNutt, 1996; Wei et al., 2015). We speculate that the presence of water facilitates low-temperature plasticity by reducing the effective activation energy for viscoelastic collapse of the microasperities at contact junctions within the fault zone, enabling the swarm-like rupture and recurrence patterns.

5. Conclusion

Although many rupture styles can readily be explained with rate- and state-dependent friction in isothermal conditions, including the thermo-mechanical coupling between shear heating and temperature-dependent friction enables a wider range of rupture styles and recurrence patterns within seismic cycles within a homogeneous asperity as temperature-hardening may lock the fault behind the rupture front. Even though many thermodynamic parameters are involved, including the activation energies for the direct weakening effect and for time-dependent healing, the heat capacity, and thermal diffusivity, a single non-dimensional parameter — the Chester-Higgs number R_h — can be used to predict the fault dynamics. For $R_h = 0$, the thermal effects have little impact on the seismic cycle and can be ignored. For a sufficiently unstable fault, a transition from crack-like to pulse-like rupture occurs for $R_h = 0.4$. In this regime, steady, decaying, and growing pulses can occur spontaneously. For increasing temperature-hardening at steady state, which is obtained either for low activation energy for the direct weakening effect or high activation enthalpy for healing, such as $0.65 \leq R_h \leq 1$, seismic swarms occur, characterized by clusters of partial ruptures that quickly break the entire seismogenic zone. Finally, for $R_h \geq 1$, the seismic cycles are characterized by tremorgenic slow-slip events occurring either sporadically or persistently, depending on the effective normal stress. Our study only explores a subset of possible physical parameters, concentrating on moderately unstable faults in condition of antiplane strain. Yet, these results plainly demonstrate that the rate-, state-, and temperature-dependent friction may help explaining a wide spectrum of dynamic rupture behaviors observed in nature.

CRediT authorship contribution statement

Conception and design of the study: Sylvain Barbot; Formal analysis: Binhao Wang; Drafting the manuscript: Binhao Wang, Sylvain Barbot.

Declaration of competing interest

The authors declare that they have no known competing financial interests or personal relationships that could have appeared to influence the work reported in this paper.

Data availability

Data will be made available on request.

Acknowledgement

We thank the editor and two anonymous reviewers for their constructive comments. We thank Han Yue for discussions on crack degree. This study is supported in part by the National Science Foundation under award number EAR-1848192.

Appendix A. Supplementary material

Supplementary material related to this article can be found online at https://doi.org/10.1016/j.epsl.2022.117983.

References

Allmann, B.P., Shearer, P.M., 2009. Global variations of stress drop for moderate to large earthquakes. J. Geophys. Res., Solid Earth 114 (B1).

An, M., Zhang, F., Elsworth, D., Xu, Z., Chen, Z., Zhang, L., 2020. Friction of Longmaxi shale gouges and implications for seismicity during hydraulic fracturing. J. Geophys. Res., Solid Earth 125 (8), e2020JB019,885. https://doi.org/10.1029/2020JB019885.

Andrews, D.J., 2002. A fault constitutive relation accounting for thermal pressurization of pore fluid. J. Geophys. Res. 107 (B12). https://doi.org/10.1029/2002JB001942. ESE–15.

Atkinson, B.K., 1984. Subcritical crack growth in geological materials. J. Geophys. Res. 89 (B6), 4077–4114.

Baba, S., Takeo, A., Obara, K., Kato, A., Maeda, T., Matsuzawa, T., 2018. Temporal activity modulation of deep very low frequency earthquakes in Shikoku, southwest Japan. Geophys. Res. Lett. https://doi.org/10.1002/2017GL076122.

Barbot, S., 2019a. Modulation of fault strength during the seismic cycle by grain-size evolution around contact junctions. Tectonophysics 765, 129–145. https://doi.org/10.1016/j.tecto.2019.05.004.

Barbot, S., 2019b. Slow-slip, slow earthquakes, period-two cycles, full and partial ruptures, and deterministic chaos in a single asperity fault. Tectonophysics 768 (228), 171. https://doi.org/10.1016/j.tecto.2019.228171.

Barbot, S., 2020. Frictional and structural controls of seismic super-cycles at the Japan trench. Earth Planets Space 72 (63). https://doi.org/10.1186/s40623-020-01185-3.

Barbot, S., 2021. A spectral boundary-integral method for quasi-dynamic ruptures of multiple parallel faults. Bull. Seismol. Soc. Am. 111 (3), 1614–1630. https://doi.org/10.1785/0120210004.

Barbot, S., 2022. A rate-, state-, and temperature-dependent friction law with competing healing mechanisms. J. Geophys. Res., e2022JB025106. https://doi.org/10.1029/2022JB025106.

Benoit, J.P., McNutt, S.R., 1996. Global volcanic earthquake swarm database and preliminary analysis of volcanic earthquake swarm duration. Ann. Geofis. 39 (2), 221.

Bizzarri, A., 2010. Pulse-like dynamic earthquake rupture propagation under rate-, state- and temperature-dependent friction. Geophys. Res. Lett. 37 (18). https://doi.org/10.1029/2010GL044541.

Blanpied, M.L., Lockner, D.A., Byerlee, J.D., 1995. Frictional slip of granite at hydrothermal conditions. J. Geophys. Res. 100 (B7), 13,045–13,064. https://doi.org/10.1029/95JB00862.

Boettcher, A., Wyllie, P., 1968. Melting of granite with excess water to 30 kilobars pressure. J. Geol. 76 (2), 235–244.

Bowden, F.P., Tabor, D., 1950. The Friction and Lubrication of Solids, Part I. Clarendon Press, Oxford.

Bowden, F.P., Tabor, D., 1964. The Friction and Lubrication of Solids, Part II. Clarendon Press, Oxford.

Bowen, N.L., 1915. The later stages of the evolution of the igneous rocks. J. Geol. 23 (S8), 1–91.

Brantley, S.L., Evans, B., Hickman, S.H., Crerar, D.A., 1990. Healing of microcracks in quartz: implications for fluid flow. Geology 18 (2), 136–139.

Brown, K.M., Fialko, Y., 2012. 'Melt welt' mechanism of extreme weakening of gabbro at seismic slip rates. Nature 488 (7413), 638. https://doi.org/10.1038/nature11370.

Chen, K., Avouac, J.-P., Aati, S., Milliner, C., Zheng, F., Shi, C., 2020. Cascading and pulse-like ruptures during the 2019 Ridgecrest earthquakes in the Eastern California Shear Zone. Nat. Commun. 11 (1), 1–8. https://doi.org/10.1038/s41467-019-13750-w.

Chester, F., Higgs, N., 1992. Multimechanism friction constitutive model for ultrafine quartz gouge at hypocentral conditions. J. Geophys. Res. 97 (B2), 1859–1870. https://doi.org/10.1029/91JB02349.

Chester, F.M., 1994. Effects of temperature on friction: constitutive equations and experiments with fault gouge. J. Geophys. Res. 99 (B4), 7247–7261. https://doi.org/10.1029/93JB03110.

Chester, F.M., 1995. A rheologic model for wet crust applied to strike-slip faults. J. Geophys. Res. 100 (B7). https://doi.org/10.1029/95JB00313. 13,033–13,044.

Coble, C., French, M., Chester, F., Chester, J., Kitajima, H., 2014. In situ frictional properties of San Andreas Fault gouge at SAFOD. Geophys. J. Int. 199 (2), 956–967. https://doi.org/10.1093/gji/ggu306.

Condit, C.B., Guevara, V.E., Delph, J.R., French, M.E., 2020. Slab dehydration in warm subduction zones at depths of episodic slip and tremor. Earth Planet. Sci. Lett. 552, 116601. https://doi.org/10.1016/j.epsl.2020.116601.

De Barros, L., Cappa, F., Deschamps, A., Dublanchet, P., 2020. Imbricated aseismic slip and fluid diffusion drive a seismic swarm in the Corinth Gulf, Greece. Geophys. Res. Lett. 47 (9), e2020GL087. https://doi.org/10.1029/2020GL087142. 142.

Di Toro, G., Goldsby, D.L., Tullis, T.E., 2004. Friction falls towards zero in quartz rock as slip velocity approaches seismic rates. Nature 427, 436–439. https://doi.org/10.1038/nature02249.

Di Toro, G., Hirose, T., Nielsen, S., Pennacchioni, G., Shimamoto, T., 2006. Natural and experimental evidence of melt lubrication of faults during earthquakes. Science 311 (5761), 647–649. https://doi.org/10.1126/science.1121012.

Di Toro, G., Han, R., Hirose, T., Paola, N.D., Nielsen, S., Mizoguchi, K., Ferri, F., Cocco, M., Shimamoto, T., 2011. Fault lubrication during earthquakes. Nature 471, 494–498. https://doi.org/10.1038/nature09838.

Dragert, H., Wang, K., James, T.S., 2001. A silent slip event on the deeper Cascadia subduction interface. Science 292 (5521), 1525–1528. https://doi.org/10.1126/science.1060152.

Dublanchet, P., De Barros, L., 2021. Dual seismic migration velocities in seismic swarms. Geophys. Res. Lett. 48 (1), e2020GL090. https://doi.org/10.1029/2020GL090025. 025.

Enomoto, Y., Yamabe, T., Okumura, N., 2017. Causal mechanisms of seismo-em phenomena during the 1965–1967 matsushiro earthquake swarm. Sci. Rep. 7 (1), 1–8.

Erickson, B., et al., 2020. The community code verification exercise for simulating Sequences of Earthquakes and Aseismic Slip (SEAS). Seismol. Res. Lett. https://doi.org/10.1785/0220190248.

French, M., Chester, F., Chester, J., 2015. Micromechanisms of creep in clay-rich gouge from the Central Deforming Zone of the San Andreas Fault. J. Geophys. Res. 120 (2), 827–849. https://doi.org/10.1002/2014JB011496.

Fukuyama, E., Hashimoto, C., Matsu'ura, M., 2002. Simulation of the transition of earthquake rupture from quasi-static growth to dynamic propagation. In: Earthquake Processes: Physical Modelling, Numerical Simulation and Data Analysis Part I. Springer, pp. 2057–2066.

Gabriel, A.-A., Ampuero, J.-P., Dalguer, L.A., Mai, P.M., 2012. The transition of dynamic rupture styles in elastic media under velocity-weakening friction. J. Geophys. Res. 117 (B9).

Goebel, T.H., Hosseini, S.M., Cappa, F., Hauksson, E., Ampuero, J.-P., Aminzadeh, F., Saleeby, J.B., 2016. Wastewater disposal and earthquake swarm activity at the southern end of the central valley, California. Geophys. Res. Lett. 43 (3), 1092–1099.

Gomberg, J., Wech, A., Creager, K., Obara, K., Agnew, D., 2016. Reconsidering earthquake scaling. Geophys. Res. Lett. 43 (12), 6243–6251.

Gu, J., Rice, J.R., Ruina, A.L., Tse, S.T., 1984. Slip motion and stability of a single degree of freedom elastic system rate and state dependent friction. J. Mech. Phys. Solids 32, 167–196.

Han, R., Shimamoto, T., Hirose, T., Ree, J.-H., Ando, J., 2007. Ultralow friction of carbonate faults caused by thermal decomposition. Science 316. https://doi.org/10.1126/science.1139763.

Hanks, T.C., Bakun, W.H., 2002. A bilinear source-scaling model for m-log a observations of continental earthquakes. Bull. Seismol. Soc. Am. 92 (5), 1841–1846.

Hawkesworth, C., Kemp, A., 2006a. The differentiation and rates of generation of the continental crust. Chem. Geol. 226 (3–4), 134–143.

Hawkesworth, C.J., Kemp, A., 2006b. Evolution of the continental crust. Nature 443 (7113), 811–817.

Heimisson, E.R., 2020. Crack to pulse transition and magnitude statistics during earthquake cycles on a self-similar rough fault. Earth Planet. Sci. Lett. 537, 116,202.

Heslot, F., Baumberger, T., Perrin, B., Caroli, B., Caroli, C., 1994. Creep, stick-slip, and dry friction dynamics: experiments and a heuristic model. Phys. Rev. E 49 (6), 4973–4988.

Higgs, N.G., 1981. Mechanical Properties of Ultrafine Quartz, Chlorite and Bentonite in Environments Appropriate to Upper-Crustal Earthquakes. Texas A &M Univ., College Station, TX. 267 pp.

Hill, R.E., Boettcher, A., 1970. Water in the Earth's mantle: melting curves of basalt-water and basalt-water-carbon dioxide. Science 167 (3920), 980–982.

Hirth, G., Tessier, C., Dunlap, W.J., 2001. An evaluation of quartzite flow laws based on comparisons between experimentally and naturally deformed rocks. Int. J. Earth Sci. 90, 77–87.

Holyoke III, C.W., Kronenberg, A.K., Newman, J., 2013. Dislocation creep of polycrystalline dolomite. Tectonophysics 590, 72–82. https://doi.org/10.1016/j.tecto.2013.01.011.

Houston, H., 2001. Influence of depth, focal mechanism, and tectonic setting on the shape and duration of earthquake source time functions. J. Geophys. Res., Solid Earth 106 (B6), 11137–11150.

Houston, H., Delbridge, B.G., Wech, A.G., Creager, K.C., 2011. Rapid tremor reversals in Cascadia generated by a weakened plate interface. Nat. Geosci. 4 (6), 404–409. https://doi.org/10.1038/ngeo1157.

Idini, B., Ampuero, J.-P., 2020. Fault-zone damage promotes pulse-like rupture and back-propagating fronts via quasi-static effects. Geophys. Res. Lett. 47 (23), e2020GL090. https://doi.org/10.1029/2020GL090736. 736.

Jiang, J., et al., 2022. Community-driven code comparisons for three-dimensional dynamic modeling of sequences of earthquakes and aseismic slip. J. Geophys. Res., Solid Earth B023, 519.

Kanamori, H., Anderson, D.L., 1975. Theoretical basis of some empirical relations in seismology. Bull. Seismol. Soc. Am. 65 (5), 1073–1095.

Kanamori, H., Brodsky, E.E., 2004. The physics of earthquakes. Rep. Prog. Phys. 67 (8), 1429.

Karato, S.-I., Jung, H., 2003. Effects of pressure on high-temperature dislocation creep in olivine. Philos. Mag. 83 (3), 401–414. https://doi.org/10.1080/0141861021000025829.

Kato, N., 2001. Effect of frictional heating on pre-seismic sliding: a numerical simulation using a rate-, state-and temperature-dependent friction law. Geophys. J. Int. 147 (1), 183–188. https://doi.org/10.1046/j.0956-540x.2001.01531.x.

Kirby, S., Kronenberg, A., 1987. Rheology of the lithosphere: selected topics. Rev. Geophys. 25 (6), 1219–1244. https://doi.org/10.1029/RG025i006p01219.

Kitajima, H., Chester, F.M., Chester, J.S., 2011. Dynamic weakening of gouge layers in high-speed shear experiments: assessment of temperature-dependent friction, thermal pressurization, and flash heating. J. Geophys. Res. 116 (B8). https://doi.org/10.1029/2010JB007879.

Kohli, A., Wolfson-Schwehr, M., Prigent, C., Warren, J.M., 2021. Oceanic transform fault seismicity and slip mode influenced by seawater infiltration. Nat. Geosci. 14 (8), 606–611.

Kronenberg, A.K., Kirby, S.H., Pinkston, J., 1990. Basal slip and mechanical anisotropy of biotite. J. Geophys. Res. 95 (B12), 19257–19278. https://doi.org/10.1029/JB095iB12p19257.

Kuna, V.M., Nábělek, J.L., Braunmiller, J., 2019. Mode of slip and crust–mantle interaction at oceanic transform faults. Nat. Geosci. 12 (2), 138–142.

Lambert, V., Lapusta, N., Perry, S., 2021. Propagation of large earthquakes as self-healing pulses or mild cracks. Nature 591 (7849), 252–258.

Liang, C., Ampuero, J.-P., Muñoz, D.P., 2022. The paucity of supershear earthquakes on large faults governed by rate and state friction. Geophys. Res. Lett., e2022GL099749.

Liu, Y., He, C., 2020. Friction properties of hornblende and implications for slow-slip events in subduction zones. Tectonophysics 796, 228. https://doi.org/10.1016/j.tecto.2020.228644. 644.

Liu, Y., Rice, J.R., 2007. Spontaneous and triggered aseismic deformation transients in a subduction fault model. J. Geophys. Res. 112 (B09404). https://doi.org/10.1029/2007JB004930.

Lohman, R., McGuire, J., 2007. Earthquake swarms driven by aseismic creep in the salton trough, California. J. Geophys. Res., Solid Earth 112 (B4).

Luo, Y., Ampuero, J.-P., 2018. Stability of faults with heterogeneous friction properties and effective normal stress. Tectonophysics 733, 257–272. https://doi.org/10.1016/j.tecto.2017.11.006.

Luo, Y., Liu, Z., 2019. Rate-and-state model casts new insight into episodic tremor and slow-slip variability in Cascadia. Geophys. Res. Lett. 46 (12), 6352–6362. https://doi.org/10.1029/2019GL082694.

Mares, V.M., Kronenberg, A., 1993. Experimental deformation of muscovite. J. Struct. Geol. 15 (9–10), 1061–1075. https://doi.org/10.1016/0191-8141(93)90156-5.

Mei, C., Barbot, S., Wu, W., 2021. Period-multiplying cycles at the transition between stick-slip and stable sliding and implications for the parkfield period-doubling tremors. Geophys. Res. Lett. L091, 807.

Meier, M.-A., Ampuero, J., Heaton, T.H., 2017. The hidden simplicity of subduction megathrust earthquakes. Science 357 (6357), 1277–1281.

Mitchell, E., Fialko, Y., Brown, K., 2016. Velocity-weakening behavior of Westerly granite at temperature up to 600 °C. J. Geophys. Res. 121 (9), 6932–6946. https://doi.org/10.1002/2016JB013081.

Mogi, K., 1963. Some discussions on aftershocks, foreshocks and earthquake swarms-the fracture of a semi-infinite body caused by an inner stress origin and its relation the earthquake phenomena. Bull. Earthq. Res. Inst. 41, 615–658.

Nakatani, M., 2001. Conceptual and physical clarification of rate and state friction: frictional sliding as a thermally activated rheology. J. Geophys. Res. 106 (B7), 13347–13380. https://doi.org/10.1029/2000JB900453.

Navrotsky, A., 1995. Thermodynamic properties of minerals. In: Mineral Physics and Crystallography: A Handbook of Physical Constants. In: AGU Ref. Shelf, vol. 2, pp. 18–28.

Nie, S., Barbot, S., 2021. Seismogenic and tremorgenic slow slip near the stability transition of frictional sliding. Earth Planet. Sci. Lett. 569, 117037. https://doi.org/10.1016/j.epsl.2021.117037.

Nie, S., Barbot, S., 2022. Rupture styles linked to recurrence patterns in seismic cycles with a compliant fault zone. Earth Planet. Sci. Lett. 591, 117593. https://doi.org/10.1016/j.epsl.2022.117593.

Nishikawa, T., Ide, S., 2017. Detection of earthquake swarms at subduction zones globally: insights into tectonic controls on swarm activity. J. Geophys. Res., Solid Earth 122 (7), 5325–5343.

Noda, H., Dunham, E.M., Rice, J.R., 2009. Earthquake ruptures with thermal weakening and the operation of major faults at low overall stress levels. J. Geophys. Res. 114 (B07302), 27. https://doi.org/10.1029/2008JB006143.

Obara, K., Kato, A., 2016. Connecting slow earthquakes to huge earthquakes. Science 353 (6296), 253–257. https://doi.org/10.1126/science.aaf1512.

Okazaki, K., Katayama, I., 2015. Slow stick slip of antigorite serpentinite under hydrothermal conditions as a possible mechanism for slow earthquakes. Geophys. Res. Lett. 42 (4), 1099–1104. https://doi.org/10.1002/2014GL062735.

Peng, Z., Gomberg, J., 2010. An integrated perspective of the continuum between earthquakes and slow-slip phenomena. Nat. Geosci. 3 (9), 599. https://doi.org/10.1038/ngeo940.

Platt, J.P., Xia, H., Schmidt, W.L., 2018. Rheology and stress in subduction zones around the aseismic/seismic transition. Prog. Earth Planet. Sci. 5 (1), 24.

Pozzi, G., De Paola, N., Nielsen, S.B., Holdsworth, R.E., Tesei, T., Thieme, M., Demouchy, S., 2021. Coseismic fault lubrication by viscous deformation. Nat. Geosci. 14 (6), 437–442. https://doi.org/10.1038/s41561-021-00747-8.

Ranjith, K., Rice, J.R., 1999. Stability of quasi-static slip in a single degree of freedom elastic system with rate and state dependent friction. J. Mech. Phys. Solids 47 (6), 1207–1218.
Rempel, A., Weaver, S., 2008. A model for flash weakening by asperity melting during high-speed earthquake slip. J. Geophys. Res. 113 (B11).
Rice, J.R., 2006. Heating and weakening of faults during earthquake slip. J. Geophys. Res. B05, 311. https://doi.org/10.1029/2005JB004006.
Rice, J.R., Ruina, A.L., 1983. Stability of steady frictional slipping. J. Appl. Mech. 50, 343–349. https://doi.org/10.1115/1.3167042.
Richet, P., Bottinga, Y., 1984. Anorthite, andesine, wollastonite, diopside, cordierite and pyrope: thermodynamics of melting, glass transitions, and properties of the amorphous phases. Earth Planet. Sci. Lett. 67 (3), 415–432. https://doi.org/10.1016/0012-821X(84)90179-1.
Richet, P., Bottinga, Y., 1986. Thermochemical properties of silicate glasses and liquids: a review. Rev. Geophys. 24 (1), 1–25. https://doi.org/10.1029/RG024i001p00001.
Rimstidt, J.D., Barnes, H., 1980. The kinetics of silica-water reactions. Geochim. Cosmochim. Acta 44 (11), 1683–1699. https://doi.org/10.1016/0016-7037(80)90220-3.
Roland, E., McGuire, J.J., 2009. Earthquake swarms on transform faults. Geophys. J. Int. 178 (3), 1677–1690. https://doi.org/10.1111/j.1365-246X.2009.04214.x.
Ross, Z.E., Cochran, E.S., 2021. Evidence for latent crustal fluid injection transients in southern California from long-duration earthquake swarms. Geophys. Res. Lett. 48 (12), e2021GL092465.
Ross, Z.E., Trugman, D.T., Azizzadenesheli, K., Anandkumar, A., 2020. Directivity modes of earthquake populations with unsupervised learning. J. Geophys. Res. 125 (2), e2019JB018299. https://doi.org/10.1029/2019JB018299.
Rousset, B., Bürgmann, R., Campillo, M., 2019a. Slow slip events in the roots of the San Andreas fault. Sci. Adv. 5 (2), eaav3274. https://doi.org/10.1126/sciadv.aav3274.
Rousset, B., Fu, Y., Bartlow, N., Bürgmann, R., 2019b. Week-long and year-long slow slip and tectonic tremor episodes on the south central Alaska megathrust. J. Geophys. Res. 122, 13–392. https://doi.org/10.1029/2019JB018724.
Rowe, C.D., Lamothe, K., Rempe, M., Andrews, M., Mitchell, T.M., Di Toro, G., White, J.C., Aretusini, S., 2019. Earthquake lubrication and healing explained by amorphous nanosilica. Nat. Commun. 10 (1), 320. https://doi.org/10.1038/s41467-018-08238-y.
Ruina, A., 1983. Slip instability and state variable friction laws. J. Geophys. Res. 88, 10359–10370. https://doi.org/10.1029/JB088iB12p10359.
Rutter, E., Brodie, K., 2004a. Experimental grain size-sensitive flow of hot-pressed Brazilian quartz aggregates. J. Struct. Geol. 26 (11), 2011–2023. https://doi.org/10.1016/j.jsg.2004.04.006.
Rutter, E., Brodie, K., 2004b. Experimental intracrystalline plastic flow in hot-pressed synthetic quartzite prepared from Brazilian quartz crystals. J. Struct. Geol. 26 (2), 259–270. https://doi.org/10.1016/S0191-8141(03)00096-8.
Rybacki, E., Dresen, G., 2000. Dislocation and diffusion creep of synthetic anorthite aggregates. J. Geophys. Res. 105 (B11), 26017–26036.
Segall, P., Rubin, A.M., Bradley, A.M., Rice, J.R., 2010. Dilatant strengthening as a mechanism for slow slip events. J. Geophys. Res. 115 (B12305). https://doi.org/10.1029/2010JB007449.
Shelly, D.R., Beroza, G.C., Ide, S., Nakamula, S., 2006. Low-frequency earthquakes in Shikoku, Japan, and their relationship to episodic tremor and slip. Nature 442, 188–191. https://doi.org/10.1038/nature04931.
Shi, Q., Barbot, S., Shibazaki, B., Matsuzawa, T., Wei, S., Tapponnier, P., 2020. Structural control and system-level behavior of the seismic cycle at the Nankai trough. Earth Planets Space 72 (1), 1–31. https://doi.org/10.1186/s40623-020-1145-0.
Strasser, F.O., Bommer, J.J., 2009. Strong ground motions—have we seen the worst? Bull. Seismol. Soc. Am. 99 (5), 2613–2637.
Sykes, L.R., 1970. Earthquake swarms and sea-floor spreading. J. Geophys. Res. 75 (32), 6598–6611.
Takahashi, M., Uehara, S.-I., Mizoguchi, K., Shimizu, I., Okazaki, K., Masuda, K., 2011. On the transient response of serpentine (antigorite) gouge to stepwise changes in slip velocity under high-temperature conditions. J. Geophys. Res. 116 (B10). https://doi.org/10.1029/2010JB008062.
Thomas, M.Y., Lapusta, N., Noda, H., Avouac, J.-P., 2014. Quasi-dynamic versus fully dynamic simulations of earthquakes and aseismic slip with and without enhanced coseismic weakening. J. Geophys. Res. 119 (3), 1986–2004. https://doi.org/10.1002/2013JB010615.
Tian, P., He, C., 2019. Velocity weakening of simulated augite gouge at hydrothermal conditions: implications for frictional slip of pyroxene-bearing mafic lower crust. J. Geophys. Res. 124 (7), 6428–6451. https://doi.org/10.1029/2018JB016456.
Toh, A., Obana, K., Araki, E., 2018. Distribution of very low frequency earthquakes in the Nankai accretionary prism influenced by a subducting-ridge. Earth Planet. Sci. Lett. 482, 342–356. https://doi.org/10.1016/j.epsl.2017.10.062.
Tse, S.T., Rice, J.R., 1986. Crustal earthquake instability in relation to the depth variation of frictional slip properties. J. Geophys. Res. 91 (B9), 9452–9472.
Valdez II, R., Kitajima, H., Saffer, D., 2019. Effects of temperature on the frictional behavior of material from the Alpine Fault Zone, New Zealand. Tectonophysics 762, 17–27. https://doi.org/10.1016/j.tecto.2019.04.022.
Veedu, D., Barbot, S., 2016. The Parkfield tremors reveal slow and fast ruptures on the same asperity. Nature 532 (7599), 361–365. https://doi.org/10.1038/nature17190.
Vidale, J.E., Shearer, P.M., 2006. A survey of 71 earthquake bursts across southern California: exploring the role of pore fluid pressure fluctuations and aseismic slip as drivers. J. Geophys. Res., Solid Earth 111 (B5).
Wang, L., Barbot, S., 2020. Excitation of San Andreas tremors by thermal instabilities below the seismogenic zone. Sci. Adv. 6 (36), eabb2057. https://doi.org/10.1126/sciadv.abb2057.
Wang, Y., Day, S.M., 2017. Seismic source spectral properties of crack-like and pulse-like modes of dynamic rupture. J. Geophys. Res., Solid Earth 122 (8), 6657–6684.
Wei, S., et al., 2015. The 2012 Brawley swarm triggered by injection-induced aseismic slip. Earth Planet. Sci. Lett. 422, 115–125. https://doi.org/10.1016/j.epsl.2015.03.054.
Wells, D.L., Coppersmith, K.J., 1994. New empirical relationships among magnitude, rupture length, rupture width, rupture area, and surface displacement. Bull. Seismol. Soc. Am. 84 (4), 975–1002.
Zheng, G., Rice, J.R., 2009. Conditions under which velocity-weakening friction allows a self-healing versus a cracklike mode of rupture. Bull. Seismol. Soc. Am. 88 (6), 1466–1483.
Zhu, W., Allison, K.L., Dunham, E.M., Yang, Y., 2020. Fault valving and pore pressure evolution in simulations of earthquake sequences and aseismic slip. Nat. Commun. 11 (1), 1–11. https://doi.org/10.1038/s41467-020-18598-z.